Acta Cryst. (1999). A**55**, 289–304

Elastic scattering of partially coherent beams of fast electrons by a crystal with a defect

N. I. Borgardt

Moscow Institute of Electronic Technology, 103498, Moscow, Russia. E-mail: lemi@mx.iki.rssi.ru

(*Received 15 January 1998; accepted 22 June 1998*)

Abstract

Scattering of a quasi-monochromatic electron beam by a crystal with a defect is described with the use of the mutual coherency function and the formalism of quasi-Bloch waves. An expression correlating the mutual intensity on the exit and entrance surfaces of the crystal in terms of the scattering matrix has been found. The matrix elements are determined by a system of integro-differential equations, which have been obtained without using the column approximation. It has been shown that calculations of the matrix elements can be significantly simplified when the approximation of the small-angle scattering of quasi-Bloch waves by the defect displacement field is satisfied. Such an approximation can be applied in many cases, *e.g.* to a crystal with a dislocation. The mutual intensity on the crystal entrance surface has been found for the general case of defocused illumination. As an example of applying the new approach, expressions for the intensity in convergent-beam electron diffraction (CBED) and large-angle CBED (LACBED) patterns have been obtained. The LACBED patterns of a crystal with a dislocation have been simulated. It has been shown that the developed approach allows a more exact simulation of the LACBED than do the conventional approaches using the column approximation and the approximation of independent plane waves filling the illumination cone.

1. Introduction

The diffraction of electrons with an energy higher than 100 keV by a crystal is usually described either with the use of the plane-wave approximation or, if the beam is convergent, with the approximation of independent plane waves incident on the specimen within the illumination cone. These approximations idealize the real electron beam that is emitted by an extended source. The coherent properties of the beam can range widely in transmission electron microscopy. The accuracy of the approximations is dependent on the influence of defects on the scattering of electrons and the conditions of both illumination and image formation. On the other hand, the approximation of coherent electron diffraction (Zuo & Spence, 1993) can only be applied to the special case of a subnanometre probe.

When high-resolution electron-microscopy images are simulated, as a rule attention is given to the effect of the incident beam convergence and the energy spread of electrons on the microscope transfer function, while, for the specimen transmission function, the approximation of a 'thin' object is used (Frank, 1973; Wade & Frank, 1977; Fejes, 1977; Hawkes, 1978; Ishizuka, 1980; Humphreys & Spence, 1981). Limitations of this approximation within the framework of the perturbation method have been investigated by Coene *et al.*, (1986). Rose (1984) proposed the use of the mutual dynamic object spectrum for describing the diffraction of electrons by the specimen under partially coherent illumination.

The independent-plane-wave approximation is used for simulating convergent-beam electron diffraction (CBED) by a perfect crystal (Spence & Zuo, 1992). Spence & Carpenter (1986) noticed that the intensity distribution on the CBED patterns is independent of the illumination coherency. A theoretical analysis validating the applicability of the approximation to the real conditions of illumination in the electron microscope has been carried out by Borgardt (1995).

The independent-plane-wave approximation is used for taking into account the incident beam convergence in simulating images of the defects. For instance, Katerbau (1981) used it to find the diffraction contrast of small dislocation loops, while Bithell *et al.* (1989) used it to calculate the stacking-fault images in a weak beam. This approximation together with the column approximation (Hirsch *et al.*, 1965) are used in simulating CBED and large-angle convergent-beam electron diffraction (LACBED) by a crystal with a defect. Carpenter & Spence (1982) calculated splitting of higher-order Laue-zone lines caused by the presence of dislocation. Bird & Preston (1988), Lu *et al.* (1990), Wang *et al.* (1992) and Chou *et al.* (1992) simulated the LACBED patterns for a crystal with a dislocation, while Wang *et al.* (1992) and Wei *et al.* (1996) simulated the LACBED patterns for a crystal with a stacking fault.

The shortcomings of the independent-plane-wave approximation in describing the scattering of a convergent electron beam lie in the fact that it takes no account of the correlations between the waves incident on the specimen at different angles. The angular size of these correlations can be comparable with a divergent angle of

wave bundles appearing after scattering a plane wave by a crystal with a defect in the directions of the transmitted and diffracted beams. Besides, the independent-plane-wave approximation does not allow the change of the incident beam coherent properties to be taken into account when the beam is focused either above or below the specimen. Recently, the applications of CBED for a local quantitative determination of deformations in a crystal have been investigated (see *e.g.* Maier *et al.*, 1996, for a review). Insufficient accuracy of the independent-plane-wave and column approximations can result in simulation errors, which would make the quantitative comparison between the experimental and simulated images difficult.

A theoretical approach allowing a description of partially coherent electron beams scattered by a perfect crystal without using the independent-plane-wave approximation has been developed by Borgardt (1993*a*, 1996). The approach involves describing the diffraction of each electron by a crystal and then taking into account the incident beam coherent properties which are characterized by the mutual coherency function and the mutual intensity function. In the present paper, the approach is developed for a crystal with a defect. In §2 an expression for mutual intensity at the exit from the crystal is obtained. Calculation of the mutual intensity on the specimen entrance surface in the general case of defocused illumination is made in §3. §4 presents an analysis of the intensity distribution in CBED and LACBED patterns and simulation of the LACBED patterns of a crystal with a dislocation.

2. Calculation of mutual intensity at the exit from the crystal

2.1. *General case*

To investigate the structure of crystals by transmission electron microscopy, a quasi-monochromatic beam is used. The average energy E_0 of electrons is equal to a hundred or more keV. The energy semiwidth of the beam, ΔE, is, as a rule, less than 1.5 eV and is dependent on the construction of the electron gun. The energy of the ith electron, E_i ($|E_i - E_0| \leq \Delta E$), is determined with the accuracy δE. The δE value is related to the time of emission of the electron by source τ_e based on the uncertainty relation $\delta E \tau_e > h$, where h is Planck's constant (Landau & Lifshitz, 1977). It is clear that δE is smaller than ΔE. The precise value of δE is not significant for further discussion.

To describe the motion of electrons, we choose the origin of the Cartesian system of coordinates at the point of intersection between the microscope optical axis and the entrance surface of the crystal, while the $0z$ axis is directed along the normal to the surface deep into the crystal. We make the origin of the coordinates in reciprocal space coincident with one of the points of the reciprocal lattice, while axes $0k_x$, $0k_y$, $0k_z$ should be parallel to the corresponding axes of the real space (Fig. 1).

The incident stationary electron beam will be characterized by the mutual coherency function, which determines the beam correlations at points $\mathbf{r}_1$ and $\mathbf{r}_2$ at the moments $t + \tau$ and t, respectively. According to the definition introduced by Borgardt (1996), it is

$$\Gamma(\mathbf{r}_1, \mathbf{r}_2, \tau) = \left\langle \sum_i \sum_{i'} \Psi(\mathbf{r}_1, t + \tau, i) \Psi^*(\mathbf{r}_2, t, i') \right\rangle, \quad (1)$$

where $\Psi(\mathbf{r}, t, i)$ is the wave function of the ith electron describing the wave package that propagates from the electron source through the specimen to the microscope screen, while $\langle\rangle$ denotes the time average.

For the quasi-monochromatic beam, the time lag τ is usually much shorter than the time of the electron beam coherency, $\tau_c = h/\Delta E$. In those cases, the expression for the mutual coherency function can be written in the form

$$\Gamma(\mathbf{r}_1, \mathbf{r}_2, \tau) = J(\mathbf{r}_1, \mathbf{r}_2) \exp(-2\pi i E_0 \tau / h), \quad (2)$$

where $J(\mathbf{r}_1, \mathbf{r}_2) = \Gamma(\mathbf{r}_1, \mathbf{r}_2, 0)$ is the mutual intensity characterizing the beam spatial coherency.

The mutual intensity function $J_c(\mathbf{r}_{c1}, \mathbf{r}_{c2})$ at points $\mathbf{r}_{c1}$ and $\mathbf{r}_{c2}$ on the crystal entrance surface is determined by the microscope illumination system. It will be calculated in §3. Calculation of mutual intensity at the exit of the specimen and then in the electron-microscopy image or in the diffraction pattern allows the average intensity $I(\mathbf{r})$ to be found by the formula

$$I(\mathbf{r}) = J(\mathbf{r}, \mathbf{r}). \quad (3)$$

To describe the mutual intensity propagation through the crystal, one should determine the relationship

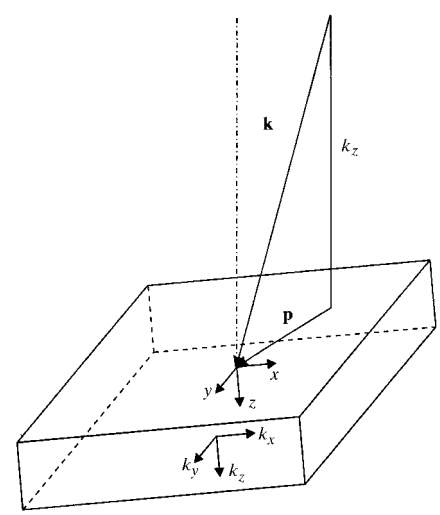

Fig. 1. Selection of the coordinate systems for describing the electron beam scattering by a crystal. The dot–dashed line represents the microscope optical axis.

between the electron wave function on its exit and entrance surfaces. We present the wave function $\Psi_V(\mathbf{r}, t, i)$ in vacuum near the crystal as a superposition of de Broglie waves,

$$\Psi_V(\mathbf{r}, t, i) = \int\int \tilde{A}(\mathbf{p}, E, i) \times \exp[2\pi i(\mathbf{k}\cdot\mathbf{r} - Et/h)]\,\mathrm{d}\mathbf{p}\,\mathrm{d}E, \quad (4)$$

where $\tilde{A}(\mathbf{p}, E, i)$ is the wave amplitude, which is non-zero at E values that are of the order of δE different from E_i, $\mathbf{k}$ is the wave vector, and $\mathbf{p}$ is the projection of vector $\mathbf{k}$ onto the plane $k_x 0 k_y$. The modulus of the vector $\mathbf{k}$, $|\mathbf{k}(E)|$, is equal to $1/\lambda(E)$, where λ is the relativistic length of the electron wave, while its k_z component is determined by the relation $k_z(\mathbf{p}, E) = [k^2(E) - p^2]^{1/2}$.

Inside the crystal, the electron wave function can be written as

$$\Psi(\mathbf{r}, t, i) = \int \Psi_S(\mathbf{r}, E, i)\exp(-2\pi i E t/h)\,\mathrm{d}E. \quad (5)$$

Functions $\Psi_S(\mathbf{r}, E, i)$ describing the stationary states with energy E can be found from the Schrödinger equation, where relativistic corrections have been introduced. In a crystal with a defect the atoms are displaced from their ideal positions. If the function $\mathbf{R}(\mathbf{r})$ describing these displacements is slowly changing at distances comparable with the lattice constant, the crystal potential can be described with the deformable ion approximation (Hirsch *et al.*, 1965). According to Borgardt (1993*b*), the solution of the Schrödinger equation with such a potential can be presented as a superposition of quasi-Bloch wave packages,

$$\Psi_S(\mathbf{r}, E, i) = \sum_j \int \psi^{(j)}(z, \mathbf{p}, E, i) b_R^{(j)}(\mathbf{p}, \mathbf{r}, E)\,\mathrm{d}\mathbf{p} \quad (6)$$

where

$$b_R^{(j)}(\mathbf{p}, \mathbf{r}, E) \equiv b_R^{(j)}(\mathbf{k}_0^{(j)}, \mathbf{r}, E) = \exp(2\pi i \mathbf{k}_0^{(j)}\cdot\mathbf{r}) \sum_g C_g^{(j)}(\mathbf{p}, E)\exp(-2\pi i R_g) \times \exp(2\pi i \mathbf{g}\cdot\mathbf{r}),$$

$R_g = \mathbf{g}\cdot\mathbf{R}(\mathbf{r})$, $b_R^{(j)}(\mathbf{p}, \mathbf{r}, E)$ is the jth quasi-Bloch wave excited in the crystal by a plane incident wave with energy E and transverse component of the wave vector $\mathbf{p}$, $\psi^{(j)}(z, \mathbf{p}, E, i)$ is the excitation amplitude of this wave, $\mathbf{k}_0^{(j)}$ is the vector with components $[p_x, p_y, k_{0z}^{(j)}(\mathbf{p}, E)]$, and $\mathbf{g}$ is a reciprocal-lattice vector.

From the definition of quasi-Bloch waves, it follows that they can be found on the basis of the Bloch-wave functions of a perfect crystal. Amplitudes $\psi^{(j)}(z, \mathbf{p}, E, i)$ describe the excitation degree of points on the branches of the dispersion surface, which is varied because of the intrabranch and interbranch scattering of quasi-Bloch waves by the displacement field of the defect when they are passing through the crystal. Variations of quasi-Bloch waves produced by inelastic scattering can be taken into account conventionally, *i.e.* by adding a small imaginary part to the k_z component of the wave vector $\mathbf{k}_0^{(j)}$. Unlike the case of a perfect crystal, the integration region in (6) cannot be selected within the two-dimensional Brillouin zone since quasi-Bloch waves are not periodical in reciprocal space. Therefore, the range of $\mathbf{p}$ vectors for which $\psi^{(j)}(z, \mathbf{p}, E, i)$ is non-zero is determined by the convergence of the incident beam and the scattering of quasi-Bloch waves by the defect displacement field.

Variations of quasi-Bloch-wave amplitudes are described by a set of integro-differential equations, which have been obtained by Borgardt (1993*b*) for the incident beam with a small convergency. As is shown in Appendix *A*, this equation set remains valid for beams with arbitrary convergency and can be written as

$$\frac{\partial\psi^{(l)}(z, \mathbf{p}, E, i)}{\partial z} = \sum_j \hat{L}_{lj}(z, E)\psi^{(j)}(z, \mathbf{p}, E, i), \quad (7)$$

where the integral operators $\hat{L}_{lj}(z, E)$ are determined by the expression

$$\begin{aligned}\hat{L}_{lj}(z, E)\psi^{(j)}(z, \mathbf{p}, E, i) &= 2\pi i \int \sum_g C^{(l)*}(\mathbf{p}, E) C_g^{(j)}(\mathbf{p}', E)(1 + g_z/K_0) \\ &\times \psi^{(j)}(z, \mathbf{p}', E, i)\exp\{2\pi i[k_{0z}^{(j)}(\mathbf{p}', E) - k_{0z}^{(l)}(\mathbf{p}, E)]z\} \\ &\times \left[\frac{\partial}{\partial z} + 2\pi i \frac{(\mathbf{p}' + \mathbf{g}_p)\cdot(\mathbf{p}' - \mathbf{p})}{K_{gz}(\mathbf{p}, E)}\right] \\ &\times \tilde{R}_g(z, \mathbf{p} - \mathbf{p}')\,\mathrm{d}\mathbf{p}',\end{aligned}$$

$$\tilde{R}_g(z, \mathbf{p}) = \int R_g(\mathbf{r})\exp(-2\pi i \mathbf{p}\cdot\boldsymbol{\rho})\,\mathrm{d}\boldsymbol{\rho},$$

$\mathbf{K}_g = \mathbf{K}_0 + \mathbf{g}$, $K_0 = [k^2(E) + U_0]^{1/2}$, U_0 is the normalized mean crystal potential, $\mathbf{g}_p$ is the projection of vector $\mathbf{g}$ onto plane $k_x 0 k_y$, $\boldsymbol{\rho}$ is the projection of the vector $\mathbf{r}$ onto plane $x0y$.

Let us divide the crystal along the $0z$ axis into N equal layers of thickness $\Delta z = z_e/N$, where z_e is the crystal thickness. Having selected point z_m in the middle of the mth layer, we can write the solution of the equation set (7) as

$$\begin{aligned}[\psi(z_e, \mathbf{p}, E, i)] = \Big\{\lim_{N\to\infty} \big([I] + \Delta z[\hat{L}(z_N, E)]\big)\ldots \\ \times \big([I] + \Delta z[\hat{L}(z_m, E]\big)\ldots \\ \times \big([I] + \Delta z[\hat{L}(z_1, E)]\big)\Big\} \\ \times [\psi(0, \mathbf{p}, E, i)],\end{aligned}$$

where $[I]$ is the unit matrix, $[\psi]$ is the column matrix with elements $\psi^{(j)}$, $[\hat{L}(z_m, E)]$ is the square matrix with the elements $\hat{L}_{lj}(z_m, E)$.

Assuming that the limit of the matrices product in the braces is existent, we obtain

$$[\psi(z_e, \mathbf{p}, E, i)] = [\hat{M}'(E)][\psi(0, \mathbf{p}, E,)i],$$

where elements of the scattering matrix $[\hat{M}']$ determine the amplitude of the lth quasi-Bloch wave as

$$\begin{aligned}\psi^{(l)}(z_e, \mathbf{p}, E, i) &= \sum_j \hat{M}'_{lj}(E)\psi^{(j)}(0, \mathbf{p}, E, i) \\ &= \sum_j \int M'_{lj}(\mathbf{p}, \mathbf{p}', E)\psi^{(j)}(0, \mathbf{p}, E, i)\,\mathrm{d}\mathbf{p}'.\end{aligned} \tag{8}$$

Amplitudes $\psi^{(j)}$ at $z = 0$ are determined by conditions on the crystal entrance surface and for them, according to Borgardt (1993*b*), we have

$$\psi^{(j)}(0, \mathbf{p}, E, i) = \tilde{A}(\mathbf{p}, E, i)C_0^{(j)*}(\mathbf{p}, E). \tag{9}$$

Expression (9) remains unchanged also when the non-zero Laue-zone reflections are taken into consideration. This is readily apparent *via* calculations, as made by Jones *et al.* (1977).

Substituting (9) into (8), we obtain

$$\psi^{(l)}(z_e, \mathbf{p}, E, i) = \int M_l(\mathbf{p}, \mathbf{p}', E)\tilde{A}(\mathbf{p}', E, i)\,\mathrm{d}\mathbf{p}', \tag{10}$$

where

$$M_l(\mathbf{p}, \mathbf{p}', E) = \sum_j M'_{lj}(\mathbf{p}, \mathbf{p}', E)C_0^{(j)*}(\mathbf{p}', E).$$

From (10), it follows that amplitudes of quasi-Bloch waves at the exit from the crystal are determined by the elements of the scattering matrix $[M]$. The elements can be found by considering the diffraction of the plane incident wave

$$\Psi_V(\mathbf{r}, E) = \exp\{2\pi i[\mathbf{p}_0 \cdot \boldsymbol{\rho} + k_z(\mathbf{p}_0, E')z - E't/h]\}.$$

Then,

$$\tilde{A}(\mathbf{p}, E, i) = \delta(\mathbf{p} - \mathbf{p}_0)\delta(E - E') \tag{11}$$

and, according to (10), we have

$$\psi^{(l)}(z_e, \mathbf{p}, E) = M_l(\mathbf{p}, \mathbf{p}_0, E)\delta(E - E') \tag{12}$$

where $\delta(x)$ is Dirac's delta function.

From expression (12), it can be seen that $M_l(\mathbf{p}, \mathbf{p}_0, E)$ describe the excitation of points on the lth branch of the dispersion surface after the scattering of the incident plane wave by the crystal. To find $M_l(\mathbf{p}, \mathbf{p}_0, E)$, it is necessary to solve the equation set (7) with the boundary conditions (11) for different $\mathbf{p}_0$ and E' values.

Using (6) and (10), for functions $\Psi_S(\mathbf{r}, E, i)$ we obtain

$$\begin{aligned}\Psi_S(\mathbf{r}, E, i) = \sum_j \int \tilde{A}(\mathbf{p}', E, i)M_j(\mathbf{p}, \mathbf{p}', E) \\ \times b_R^{(j)}(\mathbf{p}, \mathbf{r}, E)\,\mathrm{d}\mathbf{p}\,\mathrm{d}\mathbf{p}'.\end{aligned} \tag{13}$$

As δE is small, in calculating the wave function $\Psi(\mathbf{r}, t, i)$ we can assume that

$$C_g^{(j)}(\mathbf{p}, E) \simeq C_g^{(j)}(\mathbf{p}, E_i) \tag{14}$$

$$M_j(\mathbf{p}, \mathbf{p}', E) \simeq M_j(\mathbf{p}, \mathbf{p}', E_i) \tag{15}$$

$$k_{0z}^{(j)}(\mathbf{p}, E) \simeq k_{0z}^{(j)}(\mathbf{p}, E_i) + (E - E_i)/h v_z^{(j)}(\mathbf{p}, E_i) \tag{16}$$

where $v_z^{(j)} = (1/h)\partial E/\partial \mathrm{Re}(k_{0z}^{(j)})$ is the z component of the electron velocity for the jth branch while variations of the imaginary part of $k_{0z}^{(j)}$ are considered to be negligible.

Following Borgardt (1996) further, after substitution of (13) into (5) with (4), and with (14) to (16) taken into account, for the electron wave function at the point $\mathbf{r}_e$ on the crystal exit surface we find

$$\begin{aligned}\Psi(\mathbf{r}_e, t, i) = \sum_j \int\int \Psi_v[\mathbf{r}_c, t - z_e/v_z^{(j)}(\mathbf{p}, E_i), i] \\ \times M_j(\mathbf{p}, \mathbf{p}', E_i)b_R^{(j)}(\mathbf{p}, \mathbf{r}_e, E_i) \\ \times \exp[-2\pi i E_i z_e/h v_z^{(j)}(\mathbf{p}, E_i)] \\ \times \exp[-2\pi i \mathbf{p}' \cdot \boldsymbol{\rho}_c]\,\mathrm{d}\mathbf{p}\,\mathrm{d}\mathbf{p}'\,\mathrm{d}\boldsymbol{\rho}_c\end{aligned} \tag{17}$$

where $\mathbf{r}_c$ is a vector on the entrance surface of the crystal with components $(\rho_{cx}, \rho_{cy}, 0)$.

Substituting (17) into (1), assuming that relations (14) to (16) remain valid at $E = E_0$ for all electrons of the beam and taking into account that the time lag τ between any points $\mathbf{r}_{e1}$ and $\mathbf{r}_{e2}$ is much smaller than the coherency time τ_c we obtain for mutual intensity at exit from the crystal

$$\begin{aligned}J_e(\mathbf{r}_{e1}, \mathbf{r}_{e2}) = \sum_j \sum_l \int\int\int\int \tilde{J}_c(\mathbf{p}'_1, \mathbf{p}'_2)M_j(\mathbf{p}_1, \mathbf{p}'_1) \\ \times M_l^*(\mathbf{p}_2, \mathbf{p}'_2)b_R^{(j)}(\mathbf{p}_1, \mathbf{r}_{e1}) \\ \times b_R^{(l)*}(\mathbf{p}_2, \mathbf{r}_{e2})\,\mathrm{d}\mathbf{p}_1\,\mathrm{d}\mathbf{p}'_1\,\mathrm{d}\mathbf{p}_2\,\mathrm{d}\mathbf{p}'_2,\end{aligned} \tag{18}$$

where

$$\begin{aligned}\tilde{J}_c(\mathbf{p}'_1, \mathbf{p}'_2) = \int\int J_c(\mathbf{r}_{c1}, \mathbf{r}_{c2}) \\ \times \exp[-2\pi i(\mathbf{p}_1 \cdot \boldsymbol{\rho}_{c1} - \mathbf{p}_2 \cdot \boldsymbol{\rho}_{c2})]\,\mathrm{d}\boldsymbol{\rho}_{c1}\,\mathrm{d}\boldsymbol{\rho}_{c2},\end{aligned}$$

where functions depending on energy are calculated at $E = E_0$.

According to (18), $J_e(\mathbf{r}_{e1}, \mathbf{r}_{e2})$ depends on the illumination conditions determined by the function $J_c(\mathbf{r}_{c1}, \mathbf{r}_{c2})$. On the other hand, the defect displacement field influences the scattering of the electron beam. This influence is described by the elements of the scattering matrix $[M]$. In obtaining (18), only the deformable ion approximation was used. Limitations of the approximation can result in errors in descriptions of the electron scattering in a region where the displacement field $\mathbf{R}(\mathbf{r})$ is changing quickly at distances comparable with the lattice constant, *e.g.* in the vicinity of the dislocation core. These errors can influence the simulated intensity distribution in the electron microscopy images of the corresponding regions. However, they are not significant for simulating CBED or LACBED patterns of a crystal with a defect.

2.2. *Small-angle scattering of quasi-Bloch waves*

Let a plane incident wave with a transverse component $\mathbf{p}_0$ of the wave vector be diffracted by a crystal with a defect. If only the points whose transversal coordinates are close to $(\mathbf{p}_{0x}, \mathbf{p}_{0y})$ are excited on the branches of the dispersion surface when the quasi-Bloch waves are scattered, then the equation set (7) can be simplified (Borgardt, 1993*b*). In such a case, one can assume that

$$C_g^{(j)}(\mathbf{p}) \simeq C_g^{(j)}(\mathbf{p}_0) \tag{19}$$

and take into account only the linear terms in the expansion of the wave-vector k_z component into the Taylor series in the vicinity of $\mathbf{p}_0$,

$$k_{0z}^{(j)}(\mathbf{p}) \simeq k_{0z}^{(j)}(\mathbf{p}_0) + \boldsymbol{\alpha}^{(j)} \cdot (\mathbf{p} - \mathbf{p}_0), \tag{20}$$

where $\boldsymbol{\alpha}^{(j)} = \partial \mathrm{Re} k_{0z}^{(j)}/\partial \mathbf{p}$, and the variation of the imaginary part of $k_{0z}^{(j)}$ is neglected.

Introducing the excitation amplitude of the jth branch

$$\varphi^{(j)}(\mathbf{r}, \mathbf{p}_0) = \int \psi^{(j)}(z, \mathbf{p}) \exp[2\pi i(\mathbf{p} - \mathbf{p}_0) \cdot \boldsymbol{\rho}]\, \mathrm{d}\mathbf{p}, \tag{21}$$

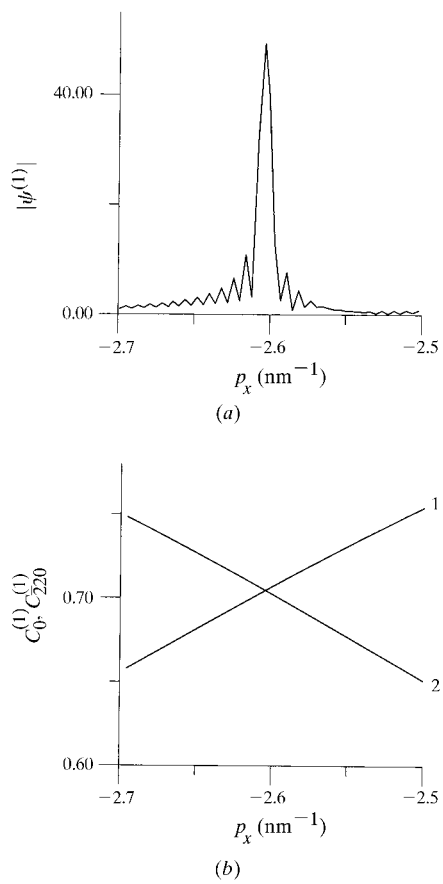

Fig. 2. (*a*) Variations of the quasi-Bloch-wave amplitude modulus $|\psi^{(1)}(z_e, p_x, 0)|$ and (*b*) coefficients $C_0^{(1)}(p_x, 0)$ (curve 1), $C_{\bar{2}20}^{(1)}(p_x, 0)$ (curve 2) in the vicinity of point $p_x = -g_{\bar{2}20}/2$.

taking into account (19), (20) and making use of the Fourier transformation properties, we obtain

$$\begin{aligned}\partial\varphi^{(l)}(\boldsymbol{\rho}, z, \mathbf{p}_0)/\partial z = 2\pi i \sum_j \sum_g & C^{(j)}(\mathbf{p}_0) C_g^{(l)*}(\mathbf{p}_0) \\ & \times (1 + g_z/K_0) \\ & \times \exp\{2\pi i[k_{0z}^{(j)}(\mathbf{p}_0) - k_{0z}^{(l)}(\mathbf{p}_0)]z\} \\ & \times \varphi^{(j)}[\boldsymbol{\rho} + (\boldsymbol{\alpha}^{(j)} - \boldsymbol{\alpha}^{(l)})z, z] \\ & \times \left[\left(\frac{\partial}{\partial z} + \boldsymbol{\theta}_g \cdot \frac{\partial}{\partial \boldsymbol{\rho}}\right) R_g(\boldsymbol{\rho} - \boldsymbol{\alpha}^{(l)} z, z)\right],\end{aligned} \tag{22}$$

where $\boldsymbol{\theta}_g = (\mathbf{p}_0 + \mathbf{g}_p)/K_{gz}(\mathbf{p}_0)$.

Expression (22) is a set of ordinary differential equations, the solution of which is considerably simpler than that of (7). Its peculiarity lies in the fact that arguments x and y of the amplitudes $\varphi^{(j)}$ on the right-hand side depend on z, while the derivations of the displacement field are calculated at point $(\boldsymbol{\rho} - \boldsymbol{\alpha}^{(l)} z, z)$.

In each particular case, the applicability of the equation set (22) can be estimated by analysing the variation of $C_g^{(j)}(\mathbf{p})$ and the effect of the neglected terms in expression (21) within the region $\Delta p_x \Delta p_y$, and the value of $\psi^{(j)}(z, \mathbf{p})$ from which the integral in expression (6) for the wave function is mainly determined. The amplitude $\psi^{(j)}(z, \mathbf{p})$, necessary for estimations, can be obtained on the basis of (21) and (22).

As an example, we consider the scattering of electrons with 100 keV energy by a silicon crystal of thickness $z_e = 150$ nm and with a surface normal $\mathbf{n}_k = [111]$, which contains an edge dislocation with the Burgers vector $\mathbf{b} = \frac{1}{2}[\bar{1}10]$ and the dislocation line $\mathbf{n}_l = [110]$. Four-beam calculations were made for systematic reflections $(\bar{2}20)$ and a plane incident wave with $p_x = -g_{\bar{2}20}/2 = -2.6$ nm^{-1}, $p_y = 0$, since the variations of $C_g^{(j)}(\mathbf{p})$ and the effect of the neglected bilinear terms in expansion (20) is maximum at the Bragg orientation of the specimen. Functions $\varphi^{(j)}(\mathbf{r})$ were determined from equation set (22), the numerical integration of which is described in §4.2. The quasi-Bloch-wave amplitudes were calculated by fast Fourier transformation.

Fig. 2 shows the dependencies of $|\psi^{(1)}(z_e, p_x, 0)|$, $C_0^{(1)}(p_x, 0)$ and $C_{\bar{2}20}^{(1)}(p_x, 0)$ with respect to p_x. From Fig. 2(*a*), it can be seen that the integral value in (6) is mainly determined by the amplitudes $\psi^{(j)}(z_e, p_x, 0)$ at p_x varying between -2.65 and -2.55 nm^{-1}. According to Fig. 2(*b*), variations of $C_0^{(1)}$ and $C_{\bar{2}20}^{(1)}$ within the range Δp_x are relatively small. Estimations also show that variations of $k_0^{(1)}(p_x, 0)$ can be significant only in a very thick crystal. Hence, approximate relations (19) and (20) have satisfactory accuracy. Therefore, for a crystal with a dislocation, considerable errors are not expected when expressions (21) and (22) are used instead of (7) for determining the quasi-Bloch-wave amplitudes $\psi^{(j)}$.

Based on (11) and (21), for the scattering matrix elements we obtain

$$M_j(\mathbf{p}, \mathbf{p}_0) = \int \varphi^{(j)}(\boldsymbol{\rho}_e, z_e, \mathbf{p}_0) \times \exp[-2\pi i(\mathbf{p} - \mathbf{p}_0) \cdot \boldsymbol{\rho}_e] \, \mathrm{d}\boldsymbol{\rho}_e. \quad (23)$$

For each $\mathbf{p}_0$, the integral value in expression (18) for the mutual intensity is mainly determined by the scattering matrix elements $M_j(\mathbf{p}, \mathbf{p}_0)$, with $\mathbf{p}$ satisfying the condition $|\mathbf{p} - \mathbf{p}_0| < |\Delta\mathbf{p}/2|$, where $\Delta\mathbf{p}$ is a vector with components $(\Delta p_x, \Delta p_y)$. As follows from the analysis of equation (22) with relations (19) and (20) taken into account, for such values of $\mathbf{p}$ one can assume the approximation

$$\varphi^{(j)}(\boldsymbol{\rho}_e, z_e, \mathbf{p}_0) \simeq \varphi^{(j)}(\boldsymbol{\rho}_e, z_e, \mathbf{p}) \quad (24)$$

when (23) is calculated.

In cases where it is possible, expressions (22) and (23) significantly simplify the determination of the scattering-matrix elements. They are used for simulating LACBED patterns in §4.

3. Mutual intensity on the crystal entrance surface

The mutual intensity on the crystal entrance surface is determined by the construction of the microscopy illumination system and the selected illumination conditions. An expression for $\tilde{J}_c(\mathbf{p}_1, \mathbf{p}_2)$ at the critical illumination of the specimen by an incoherent source filling the condenser diaphragm has been found by Borgardt (1996). However, in obtaining, for instance, LACBED patterns, the electron beam is focused either above or below the specimen entrance surface.

To calculate the mutual intensity on the crystal entrance surface for the general case, we discuss in detail the regularities of its propagation through the microscope optical system, shown schematically in Fig. 3. In order to increase the convergence angle of the incident beam and decrease its cross section in the illumination system of modern microscopes, two additional lenses L_3 and L_4 are used. The lenses are located between the condenser diaphragm and the specimen.

The condenser diaphragm behind lens L_2 is the aperture diaphragm of the microscope illumination system. It limits the angular width of the electron beam incident on the specimen. It is convenient first to calculate the mutual intensity in the plane D' located before the L_3 lens and conjugated with the plane B', which is levelled with the specimen entrance surface at its normal orientation to the microscope optical axis. Planes D' and B' are Δz_D and Δz_B distant, respectively, from planes D and B where the electron beam is focused. For illumination systems without additional lenses L_3 and L_4, which were widely used before, the D' plane is coincident with the entrance surface of the specimen.

We assume that the intermediate image of the source S_A (Fig. 3) is an effective incoherent source of electrons, *i.e.* its size is many times larger than the size of the coherency region of the electron beam in the A plane. Such an approximation is justified in the majority of cases since at a critical illumination the coherent properties of the beam incident on the specimen are dependent on the ratio between the size of the coherent region and that of the illuminated area. The size of the coherent region is determined by the condenser diaphragm radius. If, with the condenser diaphragm removed, the ratio is many times less than unity, the image of source S_A can be considered as an effective incoherent source.

For certainty, we assume that S_A is a homogeneously illuminated circle with radius d_A, though such an assumption is not obligatory for further consideration. The mutual intensity $J_A(\boldsymbol{\mu}_{A1}, \boldsymbol{\mu}_{A2})$ in the A plane can be represented as

$$J_A(\boldsymbol{\mu}_{A1}, \boldsymbol{\mu}_{A2}) = I_A \eta s_A(\mu_{A1}) \delta(\boldsymbol{\mu}_{A1} - \boldsymbol{\mu}_{A2}), \quad (25)$$

where I_A is the intensity of source S_A, $\boldsymbol{\mu}_{Ai}$ is a vector in the A plane, $s_A(\mu_A)$ is the form function, equal to one at

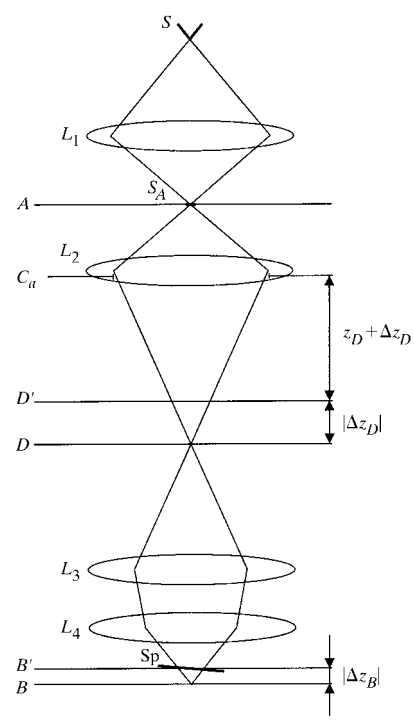

Fig. 3. The optical scheme of the specimen illumination in the electron microscope. It shows the case when $\Delta z_B < 0$. S and S_A are the electron source and its intermediate image, respectively, L_1 and L_2 are condenser lenses, L_3 is a mini-condenser lens, L_4 is an objective-condenser lens, C_a is a condenser diaphragm, and Sp the specimen.

$\mu_A \le d_A$ and to zero at other values of μ_A. Constant η has dimensions of area and determines the intensity level of the illuminated areas but does not influence the spatial structure of mutual intensity. According to Goodman (1985), we assume that $\eta = \lambda_0^2/\pi$, where $\lambda_0 = \lambda(E_0)$.

As shown by Borgardt (1996), the propagation of the electron wave mutual intensity between the optical system elements and its journey through the lens are described by formulas used in the optics of electromagnetic waves. Then, using the small-angle approximation of the Fresnel diffraction, the mutual intensity propagation from the A plane to the L_2 lens, according to Goodman (1985), is given by the expression

$$J_L(\boldsymbol{\mu}_{L1}, \boldsymbol{\mu}_{L2}) = \frac{\exp(\pi i \varphi_L)}{(\lambda_0 z_A)^2} \int\int J_A(\boldsymbol{\mu}_{A1}, \boldsymbol{\mu}_{A2}) \times \exp\left[\frac{\pi i}{\lambda_0 z_A}(\mu_{A1}^2 - \mu_{A2}^2)\right] \times \exp\left[-\frac{2\pi i}{\lambda_0 z_A}(\boldsymbol{\mu}_{L1}\cdot\boldsymbol{\mu}_{A1} - \boldsymbol{\mu}_{L2}\cdot\boldsymbol{\mu}_{A2})\right] \times \mathrm{d}\boldsymbol{\mu}_{A1}\,\mathrm{d}\boldsymbol{\mu}_{A2}, \tag{26}$$

where $\varphi_L = (\mu_{L1}^2 - \mu_{L2}^2)/\lambda_0 z_A$, z_A is the distance between the A plane and the L_2 lens, $\boldsymbol{\mu}_{Li}$ is a vector in the plane of the L_2 lens.

After substitution of (25) into (26) and integration, we obtain the well known relation (van Cittert-Zernike theorem)

$$J_L(\boldsymbol{\mu}_{L1}, \boldsymbol{\mu}_{L2}) \propto 2J_1(X)/X, \tag{27}$$

where $X = 2\pi d_A|\boldsymbol{\mu}_{L1} - \boldsymbol{\mu}_{L2}|/\lambda_0 z_A$ and $J_1(X)$ is the first-order Bessel function.

According to (27), the modulus of the mutual intensity $|J_L(\boldsymbol{\mu}_{L1}, \boldsymbol{\mu}_{L2})|$ decreases rapidly to a small value at $|\boldsymbol{\mu}_{L1} - \boldsymbol{\mu}_{L2}| > l_{sL}$, where $l_{sL} = \lambda_0 z_A/2\pi d_A$ is the coherency length of the electron beam in the plane of the L_2 lens.

The mutual intensity after passing through lens L_2 with focal distance f_L is determined by the formula

$$J'_L(\boldsymbol{\mu}_{L1}, \boldsymbol{\mu}_{L2}) = J_L(\boldsymbol{\mu}_{L1}, \boldsymbol{\mu}_{L2}) \times \exp\left[-\frac{\pi i}{\lambda_0 f_L}(\mu_{L1}^2 - \mu_{L2}^2)\right]. \tag{28}$$

Taking into account that the condenser diaphragm with the radius d_a is located in the vicinity of L_2, for mutual intensity $J_{D'}(\boldsymbol{\mu}_{D'1}, \boldsymbol{\mu}_{D'2})$ in the D' plane we obtain

$$J_{D'}(\boldsymbol{\mu}_{D'1}, \boldsymbol{\mu}_{D'2}) = \frac{\exp(\pi i \varphi_{D'})}{[\lambda_0(z_D + \Delta z_D)]^2} \int J_L(\boldsymbol{\mu}_{a1}, \boldsymbol{\mu}_{a2}) \times s_a(\mu_{a1}) s_a(\mu_{a2}) \exp\left[\frac{\pi i}{\lambda_0} \times \left(\frac{1}{z_D + \Delta z_D} - \frac{1}{f_L}\right)(\mu_{a1}^2 - \mu_{a2}^2)\right] \times \exp\left[-\frac{2\pi i}{\lambda_0(z_D + \Delta z_D)} \times (\boldsymbol{\mu}_{D'1}\cdot\boldsymbol{\mu}_{a1} - \boldsymbol{\mu}_{D'2}\cdot\boldsymbol{\mu}_{a2})\right] \mathrm{d}\boldsymbol{\mu}_{a1}\,\mathrm{d}\boldsymbol{\mu}_{a2}, \tag{29}$$

where $\varphi_{D'} = (\mu_{D'1}^2 - \mu_{D'2}^2)/\lambda_0(z_D + \Delta z_D)$, $\boldsymbol{\mu}_{a1}$ and $\boldsymbol{\mu}_{D'i}$ are vectors in the condenser diaphragm plane and in the D' plane, respectively, $s_a(\mu_a)$ is the form function, equal to one at $\mu_a \le d_a$ and zero at other values of μ_a, and z_d is the distance between the condenser diaphragm and the D plane.

The coherency length in the condenser diaphragm plane is $l_{\mathrm{sa}} \simeq l_{\mathrm{sL}} = \lambda_0 z_D/2\pi d_D$, where d_D is the illuminated circle radius in the D plane. In many cases one can assume that l_{sa} is many times smaller than the condenser diaphragm diameter (incoherent illumination). Then expression (29) can be simplified. Introducing a new variable $\boldsymbol{\mu}'_a = \boldsymbol{\mu}_{a1} - \boldsymbol{\mu}_{a2}$ we obtain

$$\mu_{a1}^2 - \mu_{a2}^2 = 2\boldsymbol{\mu}'_a\cdot\boldsymbol{\mu}_{a2} + (\mu'_a)^2$$

and

$$\boldsymbol{\mu}_{D'1}\cdot\boldsymbol{\mu}_{a1} - \boldsymbol{\mu}_{D'2}\cdot\boldsymbol{\mu}_{a2} = \boldsymbol{\mu}_{D'1}\cdot\boldsymbol{\mu}'_a + \boldsymbol{\mu}_{a2}\cdot(\boldsymbol{\mu}_{D'1} - \boldsymbol{\mu}_{D'2}).$$

Since, according to (27), function $J_L(\boldsymbol{\mu}_{a1}, \boldsymbol{\mu}_{a2})$ differs significantly from zero only at $|\boldsymbol{\mu}_{a1} - \boldsymbol{\mu}_{a2}| < l_{sL}$, we can assume that

$$s_a(\mu_{a1}) = s_a(|\boldsymbol{\mu}_{a2} + \boldsymbol{\mu}'_a|) \simeq s_a(\mu_{a2})$$

and

$$\exp\left[-\left(\frac{\pi i}{\lambda_0 z'}\right)(\mu'_a)^2\right] \simeq 1,$$

where

$$1/z' = 1/z_D - 1/(z_D + \Delta z_D).$$

With the above taken into account, after substitution of (26) into (29) we obtain

$$J_{D'}(\boldsymbol{\mu}_{D'1}, \boldsymbol{\mu}_{D'2}) = \frac{I_{\mathrm{A}}\eta \exp(\pi i \varphi_{D'})}{[\lambda_0(z_{\mathrm{D}} + \Delta z_D)]^2} \int s_a(\mu_a) \times s_D\left(\left|\frac{z_D}{z_D + \Delta z_D}\boldsymbol{\mu}_{D'1} + \frac{\Delta z_D}{z_D + \Delta z_D}\boldsymbol{\mu}_a\right|\right) \times \exp\left[-\frac{2\pi i}{\lambda_0(z_D + \Delta z_D)} \times \boldsymbol{\mu}_a\cdot(\boldsymbol{\mu}_{D'1} - \boldsymbol{\mu}_{D'2})\right] \mathrm{d}\boldsymbol{\mu}_a, \tag{30}$$

where $s_D(\mu) = s_A(\mu z_A/z_D)$ is the form function of illuminated area in the D plane.

The expression determines the electron beam mutual intensity in the D' plane distant from the D plane where the electron beam is focused. At $\Delta z_D = 0$ the size of the illuminated area, *i.e.* the range of $\boldsymbol{\mu}_{D'1}$ in which $J_{D'}(\boldsymbol{\mu}_{D'1}, \boldsymbol{\mu}_{D'2})$ is non-zero, is determined by the function $s_D(\mu_{D'1})$. In this case, the coherency length $l_{sD} = \lambda_0 z_D/2\pi d_a$ is determined by the size of the condenser diaphragm and is the same for the whole illuminated area.

At $\Delta z_D \neq 0$, mutual intensity is non-zero at $\boldsymbol{\mu}_{D'1}$, for which form functions s_D and s_a have a region in common. The values of $\boldsymbol{\mu}_{D'1}$ determining the illuminated area are given by the formula

$$\mu_{D'1} \leq \frac{|\Delta z_D|}{z_D}\left(d_a + \frac{\Delta z_D}{|\Delta z_D|} d_D\right) + d_D \simeq \frac{|\Delta z_D|}{z_D} d_a + d_D = d_{D'},$$

where we took into account that $d_a \gg d_D$, while $d_{D'}$ is the radius of the illuminated circle in the D' plane.

At $\Delta z_D \neq 0$, function $J_{D'}(\boldsymbol{\mu}_{D'1}, \boldsymbol{\mu}_{D'2})$ and, hence, the coherence length became different at different points of the illuminated area. For central points, mutual intensity can be calculated analytically by considering two cases.

In the first case, $\Delta z_D \leq z_D d_D/d_a$ or $d_{D'} \leq 2d_D$. For points $\boldsymbol{\mu}_{D'1}$ satisfying the condition

$$|\boldsymbol{\mu}_{D'1}| \leq 2d_D - d_{D'}, \tag{31}$$

the integration region in expression (30) is determined by the function s_a, and for $J_{D'}(\boldsymbol{\mu}_{D'1}, \boldsymbol{\mu}_{D'2})$ we obtain

$$J_{D'}(\boldsymbol{\mu}_{D'1}, \boldsymbol{\mu}_{D'2}) = \frac{I_A \eta \pi d_a^2 \exp(\pi i \varphi_{D'})}{[\lambda_0(z_D + \Delta z_D)]^2} \frac{2J_1(X_1)}{X_1}, \tag{32}$$

where $X_1 = 2\pi d_a |\boldsymbol{\mu}_{D'1} - \boldsymbol{\mu}_{D'2}|/\lambda_0(z_D + \Delta z_D)$.

Since the value of $(z_D + \Delta z_D)$ determines the distance between the condenser diaphragm and the D' plane, formula (32) is similar to the expression for the mutual intensity of the focused beam, while the coherency length $l_{sD'} = \lambda_0(z_D + \Delta z_D)/2\pi d_a$ is increased or decreased depending on the sign of Δz_D.

In the second case, $\Delta z_D > z_D d_D/d_a$ or $d_{D'} > 2d_D$. In this case, at points $\boldsymbol{\mu}_{D'1}$ for which

$$|\boldsymbol{\mu}_{D'1}| \leq d_{D'} - 2d_D \tag{33}$$

after integration, we obtain

$$J_{D'}(\boldsymbol{\mu}_{D'1}, \boldsymbol{\mu}_{D'2}) = \frac{I_A \eta \pi d_D^2 \exp(\pi i \varphi_{D'})}{(\lambda_0 \Delta z_D)^2} \times \exp\left[\frac{2\pi i (d_a + d_D \Delta z_D/|\Delta z_D|)}{\lambda_0(z_D + \Delta z_D)(d_{D'} - d_D)} \times \boldsymbol{\mu}_{D'1} \cdot (\boldsymbol{\mu}_{D'1} - \boldsymbol{\mu}_{D'2})\right] \frac{2J_1(X_2)}{X_2}, \tag{34}$$

where $X_2 = 2\pi d_D |\boldsymbol{\mu}_{D'1} - \boldsymbol{\mu}_{D'2}|/\lambda_0 \Delta z_D$.

From (34), it follows that, at sufficiently large Δz_D values, the coherency length $l_{sD'} = \lambda_0 \Delta z_D/2\pi d_D$ in the central region is determined by the angular size of the focused electron beam with respect to the intersection point of the microscope optical axis and the D' plane. The conclusion is in agreement with the results obtained by Pozzi (1987), who used the Gaussian function both for modelling the intensity of the effective incoherent electron source and for the transmission function of the condenser diaphragm. At peripheral points of the illuminated area which do not satisfy conditions (31) and (33), the mutual intensity in both cases can be calculated by a numerical integration of (30).

According to (18), the mutual intensity at the exit from the crystal is determined by the mutual intensity Fourier transform on its entrance surface. To find $\tilde{J}_c(\mathbf{p}_1, \mathbf{p}_2)$, it is reasonable first to calculate the Fourier transform of mutual intensity $\tilde{J}_{D'}(\mathbf{p}_1, \mathbf{p}_2)$ in the D' plane. To obtain $\tilde{J}_{D'}(\mathbf{p}_1, \mathbf{p}_2)$, we make the Fourier transformation of (30):

$$\tilde{J}_{D'}(\mathbf{p}_1, \mathbf{p}_2) = \frac{I_A \eta}{[\lambda_0(z_D + \Delta z_D)]^2} \int\int\int s_a(\mu_a) \times s_D\left(\left|\frac{z_D}{z_D + \Delta z_D}\boldsymbol{\mu}_{D'1} + \frac{\Delta z_D}{z_D + \Delta z_D}\boldsymbol{\mu}_a\right|\right) \times \exp\left[\frac{\pi i}{\lambda_0(z_D + \Delta z_D)}(\mu_{D'1}^2 - \mu_{D'2}^2)\right] \times \exp\left[-\frac{2\pi i}{\lambda_0(z_D + \Delta z_D)} \times \boldsymbol{\mu}_a \cdot (\boldsymbol{\mu}_{D'1} - \boldsymbol{\mu}_{D'2})\right] \exp[-2\pi i \times (\mathbf{p}_1 \cdot \boldsymbol{\mu}_{D'1} - \mathbf{p}_2 \cdot \boldsymbol{\mu}_{D'2})]\, \mathrm{d}\boldsymbol{\mu}_a\, \mathrm{d}\boldsymbol{\mu}_{D'1}\, \mathrm{d}\boldsymbol{\mu}_{D'2}. \tag{35}$$

Introducing a new variable $\boldsymbol{\mu}'_{D'} = \boldsymbol{\mu}_{D'1} - \boldsymbol{\mu}_{D'2}$, we have

$$\mu_{D'1}^2 - \mu_{D'2}^2 = 2\boldsymbol{\mu}'_{D'} \cdot \boldsymbol{\mu}_{D'1} - (\mu'_{D'})^2$$
$$\mathbf{p}_1 \cdot \boldsymbol{\mu}_{D'1} - \mathbf{p}_2 \cdot \boldsymbol{\mu}_{D'2} = \mathbf{p}_2 \cdot \boldsymbol{\mu}'_{D'} + (\mathbf{p}_1 - \mathbf{p}_2) \cdot \boldsymbol{\mu}_{D'1}.$$

From (32) and (34), it follows that the range of values $|\boldsymbol{\mu}_{D'1} - \boldsymbol{\mu}_{D'2}|$ at which the integrand in (35) is non-zero has the same value order as the coherence length. Hence, at the real value of z_d and with not too large a value of Δz_D, the relation $\exp\{-[\pi i/\lambda_0(z_D + \Delta z_D)](\mu'_{D'1})^2\} \simeq 1$ is satisfied.

With the above taken into account, we obtain

$$\tilde{J}_{D'}(\mathbf{p}_1, \mathbf{p}_2) = I_A \eta \int s_a[|\boldsymbol{\mu}_{D'1} - \lambda(z_D + \Delta z_D)\mathbf{p}_2|] \times s_D(|\boldsymbol{\mu}_{D'1} - \lambda \Delta z_D \mathbf{p}_2|) \times \exp[-2\pi i (\mathbf{p}_1 - \mathbf{p}_2) \cdot \boldsymbol{\mu}_{D'1}]\, \mathrm{d}\boldsymbol{\mu}_{D'1}. \tag{36}$$

Expression (36) is non-zero if the two circles determined by functions s_a and s_D have a region in common. Therefore, vectors $\mathbf{p}_2$, for which $\tilde{J}_{D'}(\mathbf{p}_1, \mathbf{p}_2) \neq 0$ must satisfy the condition

$$p_2 \leq \frac{d_a}{\lambda_0 z_D} + \frac{d_D}{\lambda_0 z_D} \simeq \frac{\theta_D}{\lambda_0}, \quad (37)$$

where $\theta_D = d_a/z_D$.

Making the substitution $\boldsymbol{\mu}_{D'} = \boldsymbol{\mu}_{D'1} - \lambda_0 \Delta z_D \mathbf{p}_2$ and having in mind that for almost all allowable vectors $\mathbf{p}_2$ the integration region in (36) is determined by function s_D, we finally have

$$\tilde{J}_{D'}(\mathbf{p}_1, \mathbf{p}_2) = I_A \eta \pi d_D^2 \tilde{S}_D(p_2) \times \exp[2\pi i \lambda \Delta z_D \mathbf{p}_2 \cdot (\mathbf{p}_1 - \mathbf{p}_2)] \times [2J_1(2\pi d_D |\mathbf{p}_1 - \mathbf{p}_2|)/2\pi d_D |\mathbf{p}_1 - \mathbf{p}_2|], \quad (38)$$

where $\tilde{S}_D(p)$ is the form function in reciprocal space which appears according to (37). It equals one at $p \leq \theta_D/\lambda_0$ and zero at other values of p.

Now we calculate the mutual intensity and its Fourier transform in the B' plane. Since the exit pupil of the microscope illumination system is determined by the size of the condenser diaphragm, then, neglecting the aberrations of lenses L_3 and L_4 and taking into account Hawkes (1978), we have for mutual intensity in the B' plane

$$J_{B'}(\boldsymbol{\mu}_{B'1}, \boldsymbol{\mu}_{B'2}) = (1/\Gamma_M^2) J_{D'}(\boldsymbol{\mu}_{B'1}/\Gamma_M, \boldsymbol{\mu}_{B'2}/\Gamma_M), \quad (39)$$

where $\boldsymbol{\mu}_{B'i}$ is the vector in the B' plane and Γ_M is the magnification coefficient of the optical system made up of lenses L_3 and L_4.

By using formulas (26) and (28), one can directly see that (39) is valid. Expression (39) allows the mutual intensity in the B' plane to be determined on the basis of (30), (32) and (34) and taking into account that

$$d_{B'} = \Gamma_M d'_D, \quad (40)$$

where $d_{B'}$ is the radius of the illuminated circle in the B' plane.

The relation between $\Delta z_{D'}$ and $\Delta z_{B'}$ can be found with the help of Maxwell's elongation formula (Born & Wolf, 1968). For small Δz_B values, it is

$$\Delta z_B \simeq \Delta z_D \Gamma_M^2. \quad (41)$$

Based on formulas (38) to (41) for the Fourier transform $\tilde{J}_{B'}(\mathbf{p}_1, \mathbf{p}_2)$, we obtain

$$\tilde{J}_{B'}(\mathbf{p}_1, \mathbf{p}_2) = I_A \eta \pi d_B^2 \tilde{S}_B(p_2) \times \exp[-2\pi i \lambda \Delta z_B \mathbf{p}_2 \cdot (\mathbf{p}_1 - \mathbf{p}_2)] \times [2J_1(2\pi d_B |\mathbf{p}_1 - \mathbf{p}_2|)/2\pi d_B |\mathbf{p}_1 - \mathbf{p}_2|], \quad (42)$$

where $\tilde{S}_B(p) = \tilde{S}_D(p\Gamma_M)$, $\tilde{S}_B(p)$ is equal to unity at $p \leq \theta_B/\lambda_0$ and zero at other values of p, θ_B is the semi-angle of the incident beam convergency.

From (42), it follows that in the expression for $\tilde{J}_{B'}(\mathbf{p}_1, \mathbf{p}_2)$ an additional phase factor appears when the B' plane is distant from the B plane where an electron beam is focused. The importance of the factor increases with increasing $|\Delta z_B|$.

In the above analysis, it has been assumed that the L_2 condenser lens forms a real image of the electron source. To minimize the cross section of the focused beam, the L_2 lens can be excited slightly while the L_3 lens is not excited at all (*e.g.* in the nanoprobe mode for modern Philips microscopes). Then the L_2 lens forms a virtual image of the source. In this case, the mutual intensity and its Fourier transform in the B' plane can also be calculated using (30), (39) and (42), respectively, since functions $J_{D'}(\boldsymbol{\mu}_{D'1}, \boldsymbol{\mu}_{D'2})$ and $\tilde{J}_{D'}(\mathbf{p}_1, \mathbf{p}_2)$ in the plane of virtual images are formally described by (30) and (38).

Expressions (30), (39) and (42) directly determine the mutual intensity $J_c(\boldsymbol{\rho}_{c1}, \boldsymbol{\rho}_{c2})$ and its Fourier transform $\tilde{J}_c(\mathbf{p}_1, \mathbf{p}_2)$ on the entrance surface of the specimen when it is oriented to be normal to the microscope optical axis. At small deviations from the normal orientation, $J_c(\boldsymbol{\rho}_{c1}, \boldsymbol{\rho}_{c2})$ can be calculated on the basis of the formula for $J_{B'}(\boldsymbol{\mu}_{B'1}, \boldsymbol{\mu}_{B'2})$ by introducing a phase factor (see *e.g.* Borgardt, 1996).

4. Simulation of a LACBED pattern

4.1. *Intensity distribution in the diffraction pattern*

Analysing the intensity distribution in diffraction patterns, we consider a typical case of a plane-parallel crystal oriented perpendicular to the microscopy optical axis. Using (26) and (28), one can easily obtain an expression correlating the mutual intensity $J_f(\boldsymbol{\mu}_{f1}, \boldsymbol{\mu}_{f2})$ in the rear focal plane of the objective lens with that on the crystal exit surface. The expression is well known in optics (Goodman, 1985) and has the form

$$J_f(\boldsymbol{\mu}_{f1}, \boldsymbol{\mu}_{f2}) = [\exp(\pi i \varphi_f)/(\lambda_0 f)^2] \int J_e(\boldsymbol{\rho}_{e1}, \boldsymbol{\rho}_{e2}) \times \exp[-(2\pi i/\lambda_0 f) \times (\boldsymbol{\rho}_{e1} \cdot \boldsymbol{\mu}_{f1} - \boldsymbol{\rho}_{e2} \cdot \boldsymbol{\mu}_{f2})] \, \mathrm{d}\boldsymbol{\rho}_{e1} \, \mathrm{d}\boldsymbol{\rho}_{e2}, \quad (43)$$

where $\varphi_f = (1 - z_o/f)(\mu_{f1}^2 - \mu_{f2}^2)/\lambda_0 f$, z_o is the distance between the specimen and the objective lens, and f is the focal distance of the objective lens.

Henceforth, for simplicity, we will limit ourselves to discussion of diffraction patterns in which the neighbouring discs are not overlapped. For CBED patterns, such a situation does not arise if the convergency semi-angle of the incident beam is smaller than the minimal one among the Bragg angles. For LACBED patterns, overlap of the neighbouring discs is avoided by introducing the selector diaphragm. After substitution of (18) into (43) and taking (3) into account for the transmitted beam intensity in the rear focal plane of the objective lens, we have

$$I_f(\boldsymbol{\mu}_f) = \sum_j \sum_l \int\int \tilde{J}_c(\mathbf{p}_1, \mathbf{p}_2) F^{(jl)}(\mathbf{q}_f) M_j(\mathbf{q}_f, \mathbf{p}_1) \times M_l^*(\mathbf{q}_f, \mathbf{p}_2) \, \mathrm{d}\mathbf{p}_1 \, \mathrm{d}\mathbf{p}_2, \quad (44)$$

where

$$F^{(jl)}(\mathbf{q}_f) = [1/(\lambda_0 f)^2] C_0^{(j)}(\mathbf{q}_f) C_0^{(l)*}(\mathbf{q}_f) \times \exp\{2\pi i [k_{0z}^{(j)}(\mathbf{q}_f) - k_{0z}^{(l)*}(\mathbf{q}_f)] z_e\}$$

and $\mathbf{q}_f = \boldsymbol{\mu}_f/\lambda_0 f$.

To make the physical sense of expression (44) clearer, we will consider the case of incoherent critical illumination. According to (42), at $\Delta z_B = 0$ we have

$$\tilde{J}_c(\mathbf{p}_1, \mathbf{p}_2) \propto \tilde{S}_B(p_2) \frac{2J_1(2\pi d_B|\mathbf{p}_1 - \mathbf{p}_2|)}{2\pi d_B|\mathbf{p}_1 - \mathbf{p}_2|}. \quad (45)$$

After substitution of (45) into (44), we obtain

$$I_f(\boldsymbol{\mu}_f) \propto \sum_j \sum_l \int \tilde{S}_B(p_2) F^{(jl)}(\mathbf{q}_f) M_j(\mathbf{q}_f, \mathbf{p}_1) M_l^*(\mathbf{q}_f, \mathbf{p}_2) \times \frac{2J_1(2\pi d_B|\mathbf{p}_1 - \mathbf{p}_2|)}{2\pi d_B|\mathbf{p}_1 - \mathbf{p}_2|} \, \mathrm{d}\mathbf{p}_1 \, \mathrm{d}\mathbf{p}_2. \quad (46)$$

From (46), one can see that the intensity at point $\boldsymbol{\mu}_f = \lambda_0 f \mathbf{q}_f$ in the diffraction pattern is contributed to by all the plane waves incident on the crystal. The contributions of waves with different wave vectors are determined both by the scattering matrix elements $M_j(\mathbf{q}_f, \mathbf{p})$ and by correlations between the incident waves. Matrix elements $M_j(\mathbf{q}_f, \mathbf{p})$ depend on the conditions of the quasi-Bloch waves scattering by the displacement field of the defect. At large values of the modulus $|\mathbf{q}_f - \mathbf{p}|$, modulus $|M_j(\mathbf{q}_f, \mathbf{p})|$ rapidly becomes small. Under the critical illumination, correlations between plane waves with different wave vectors are determined by the cross section of the electron probe. When the independent-plane-wave approximation is used, these correlations are not taken into account, *i.e.* it is assumed that

$$\tilde{J}_c(\mathbf{p}_1, \mathbf{p}_2) \propto \tilde{S}_B(p_2) \delta(\mathbf{p}_1 - \mathbf{p}_2).$$

According to (45), this relation is valid if the illuminated area on the entrance surface of the specimen is sufficiently large.

Calculation of intensity $I_f(\boldsymbol{\mu}_f)$ based on the general formula (44) requires solving equations (7) for a large number of $\mathbf{q}_f$ and $\mathbf{p}$ values. If the scattering angles of quasi-Bloch waves by the displacement field of the defect are small, calculations can be considerably reduced by using (22) and (23) for determining $M_j(\mathbf{q}_f, \mathbf{p})$. Then, expressing the Fourier transform $\tilde{J}_c(\mathbf{p}_1, \mathbf{p}_2)$ in terms of the mutual intensity function $J_c(\mathbf{r}_{c1}, \mathbf{r}_{c2})$, substituting (23) into (44) and taking (24) into account, we obtain

$$I_f(\boldsymbol{\mu}_f) = \sum_j \sum_l \int\int J_c(\boldsymbol{\rho}_{e1}, \boldsymbol{\rho}_{e2}) F^{(jl)}(\mathbf{q}_f) \varphi^{(j)}(\boldsymbol{\rho}_{e1}, z_e, \mathbf{q}_f) \times \varphi^{(l)*}(\boldsymbol{\rho}_{e2}, z_e, \mathbf{q}_f) \times \exp[-2\pi i \mathbf{q}_f \cdot (\boldsymbol{\rho}_{e1} - \boldsymbol{\rho}_{e2})] \, \mathrm{d}\boldsymbol{\rho}_{e1} \, \mathrm{d}\boldsymbol{\rho}_{e2}. \quad (47)$$

Equations (44) and (47) describe the intensity in the diffraction pattern in the general case of partially coherent illumination. Further simplification of the expression for $I_f(\boldsymbol{\mu}_f)$ is possible at incoherent illumination. Then, using expression (42) for the Fourier transform of mutual intensity and (23) and (24) for $M_j(\mathbf{q}_f, \mathbf{p}_1)$, after integration in (44) we have

$$I_f(\boldsymbol{\mu}_f) = I_A \eta \pi d_B^2 \tilde{S}_B(q_f) \sum_j \sum_l F^{(jl)}(\mathbf{q}_f) \times \int\int \varphi^{(j)}(\boldsymbol{\rho}_e - \lambda_0 \Delta z_B \mathbf{p}, z_e, \mathbf{q}_f) \varphi^{(l)*}(\boldsymbol{\rho}_e, z_e, \mathbf{q}_f) \times \exp[-2\pi i \mathbf{p} \cdot (\boldsymbol{\rho}_e - \lambda_0 \Delta z_B \mathbf{q}_f)] \times \exp(2\pi i \lambda \Delta z_B p^2)[2J_1(2\pi d_B p)/2\pi d_B p] \, \mathrm{d}\boldsymbol{\rho}_e \, \mathrm{d}\mathbf{p}. \quad (48)$$

Expression (48) describes the intensity distribution in the diffraction pattern when the electron beam is defocused. For CBED patterns at $\Delta z_B = 0$, it can be presented in the form

$$I_f(\boldsymbol{\mu}_f) = I_A \eta \tilde{S}_B(q_f) \sum_j \sum_l F^{(jl)}(\mathbf{q}_f) \int \varphi^{(j)}(\boldsymbol{\rho}_e, z_e, \mathbf{q}_f) \times \varphi^{(l)*}(\boldsymbol{\rho}_e, z_e, \mathbf{q}_f) s_B(\rho_e) \, \mathrm{d}\boldsymbol{\rho}_e \quad (49)$$

where $s_B(\mu) = s_D(\mu/\Gamma_M)$.

From (49), it follows that for calculating the intensity in the CBED patterns it is sufficient to find amplitudes $\varphi^{(j)}$ on the crystal exit surface within the area determined by the cross section of the focused electron beam. If calculation of $\varphi^{(j)}$ is made with the column approximation, *i.e.* we assume that $\boldsymbol{\alpha}^{(j)} = 0$ and $\boldsymbol{\theta}_g = 0$ when (22) is solved (Borgardt, 1993*b*), for intensity $I_f(\boldsymbol{\mu}_f)$ we obtain

$$I_f(\boldsymbol{\mu}_f) = [I_A \eta \tilde{S}_B(q_f)/(\lambda_0 f)^2] \int I_0(\boldsymbol{\rho}_e, z_e, \mathbf{q}_f) s_B(\rho_e) \, \mathrm{d}\boldsymbol{\rho}_e, \quad (50)$$

where $I_0(\boldsymbol{\rho}_e, z_e, \mathbf{q}_f)$ is the intensity of the transmitted electron wave at point $(\boldsymbol{\rho}_e, z_e)$, produced by the plane incident wave with the transverse component of the wave vector $\mathbf{q}_f$ and which is calculated with the column approximation.

For LACBED patterns after integration over $\boldsymbol{\rho}_e$ in (48), the range of $\mathbf{p}$ values at which the integrand is nonzero is the same as for the function $M_j(\mathbf{q}_f + \mathbf{p}, \mathbf{q}_f)$. Since the typical value of d_B is of the order of a few nanometers, for many defects one can assume that

$$2J_1(2\pi d_B p)/2\pi d_B p \simeq 1$$

at all $\mathbf{p}$ for which the expression under the integral sign in (48) differs from zero. Then, making a substitution of variables

$$\mathbf{p}' = [\boldsymbol{\rho}_e - \lambda_0 \Delta z_B (\mathbf{p} + \mathbf{q}_f)]/\lambda_0 \Delta z_B,$$

we present $I_f(\boldsymbol{\mu}_f)$ as

$$I_f(\boldsymbol{\mu}_f) = I_A \eta \pi d_B^2 \tilde{S}_B(q_f) \sum_j \sum_l F^{(jl)}(\mathbf{q}_f) \times \int\int \varphi^{(j)}[\lambda_0 \Delta z_B (\mathbf{q}_f + \mathbf{p}'), z_e, \mathbf{q}_f] \varphi^{(l)*}(\boldsymbol{\rho}_e, z_e, \mathbf{q}_f) \times \exp[-2\pi i \mathbf{p}' \cdot (\boldsymbol{\rho}_e - \lambda \Delta z_B \mathbf{q}_f)] \times \exp[2\pi i \lambda \Delta z_B (p')^2] \, \mathrm{d}\boldsymbol{\rho}_e \, \mathrm{d}\mathbf{p}'. \quad (51)$$

Using expression (51) instead of (48) simplifies simulation of intensity since a numerical integration can be made by fast Fourier transformation, which allows the calculation time to be considerably reduced. If $|\Delta z_B|$ is sufficiently small, the influence of the factor quadratic in $\mathbf{p}'$ in (51) is negligible and we can assume that

$$\varphi^{(j)}[\lambda_0\Delta z_B(\mathbf{q}_f+\mathbf{p}'), z_e, \mathbf{q}_f] \simeq \varphi^{(j)}(\lambda_0\Delta z_B\mathbf{q}_f, z_e, \mathbf{q}_f). \tag{52}$$

Besides, if amplitudes $\varphi^{(j)}$ are determined with the column approximation, we obtain for intensity

$$I_f(\boldsymbol{\mu}_f) = [I_A\eta\pi d_B^2/(\lambda_0 f)^2]\tilde{S}_B(q_f)I_0(\lambda_0\Delta z_B\mathbf{q}_f, z_e, \mathbf{q}_f). \tag{53}$$

Formula (53) was used by Bird & Preston (1988), Lu *et al.* (1990), Wang *et al.* (1992) and Chou *et al.* (1992) for simulating LACBED patterns of a crystal with a dislocation. Errors arising in this case will be discussed in §4.3.

4.2. *Information localization and shortcomings of conventional approximations*

Expressions (49) and (51) make it possible to estimate the cross size $\Delta\rho$ of the crystal region that influences the intensity at point $\boldsymbol{\mu}_f = \lambda_0\Delta z_B\mathbf{q}_f$ in the diffraction pattern. This size determines the information localization when the displacement field is investigated by means of convergent-beam diffraction. Based on (49), $\Delta\rho$ for CBED patterns can be presented as

$$\Delta\rho(\mathbf{q}_f) = \Delta\rho_{\rm cr}(\mathbf{q}_f) + d_B, \tag{54}$$

where $\Delta\rho_{\rm cr}(\mathbf{q}_f) = z_e\max[|\boldsymbol{\alpha}^{(j)}(\mathbf{q}_f) - \boldsymbol{\alpha}^{(l)}(\mathbf{q}_f)|]$, in which 'max' denotes the maximum value of the difference at various j's and l's.

Estimation of $\Delta\rho_{\rm cr}$ follows directly from the analysis of (22). $\Delta\rho_{\rm cr}$ appears in the right-hand part of (54) because of the fact that quasi-Bloch packages transfer the disturbances perpendicular to the excited sections of the dispersion surface (Borgardt, 1993*b*). This is shown schematically in Fig. 4 for a wave with transverse component of the wave vector $\mathbf{q}_f$. In passing through the defective region of the crystal, the quasi-Bloch waves are scattered, and as a result the diffuse background appears at the crystal exit. When the column approximation is used, the inclination of the excited parts of the dispersion surface is neglected [$\boldsymbol{\alpha}^{(j)}(\mathbf{q}_f) = 0$] and, hence, the spatial separation of the wave fields corresponding to different branches of the dispersion surface is not taken into account. Therefore, the accuracy of this approximation is dependent on the values of $\boldsymbol{\alpha}^{(j)}(\mathbf{q}_f)$. If the values of $\boldsymbol{\alpha}^{(j)}(\mathbf{q}_f)$ are non-zero, the column-approximation errors are increased when the region of a strong scattering of quasi-Bloch waves, *e.g.* the dislocation core, becomes more distant from the crystal entrance surface. The column-approximation errors are decreased when the defect is displaced in the lateral direction with respect to the illuminated area.

It is noteworthy that, in simulating electron microscopy images formed by a beam with a small convergency, the column-approximation accuracy is increased when the defect becomes more distant from the crystal entrance surface (Borgardt, 1993*b*).

For LACBED patterns with $|\Delta z_B|$ increasing, the exponential factor which is quadratic in $\mathbf{p}'$ becomes significant. This factor is responsible for an additional term in the expression for $\Delta\rho$. To evaluate $\Delta\rho$ in that case we use the approximate relation (52). Then, for $I_f(\boldsymbol{\mu}_f)$ we have

$$\begin{aligned} I_f(\boldsymbol{\mu}_f) \propto \sum_j\sum_l F^{(jl)}(\mathbf{q}_f)\varphi^{(j)}[\lambda_0\Delta z_B\mathbf{q}_f, z_e, \mathbf{q}_f] \\ \times \{\varphi^{(l)^*}(\lambda_0\Delta z_B\mathbf{q}_f, z_e, \mathbf{q}_f) \\ * \exp[-\pi i(\lambda_0\Delta z_B\mathbf{q}_f)^2/2\lambda_0\Delta z_B]\}, \end{aligned} \tag{55}$$

where $*$ denotes the convolution operation. Since the result of convolution is mainly determined by the values of function $\varphi^{(l)}$ at points $\boldsymbol{\rho}$, for which

$$(\boldsymbol{\rho} - \lambda_0\Delta z_B\mathbf{q}_f)^2/2\lambda_0\Delta z_B \lesssim 1,$$

we obtain

$$\Delta\rho(\mathbf{q}_f) \simeq \Delta\rho_{\rm cr}(\mathbf{q}_f) + d_B + 2(2\lambda_0\Delta z_B)^{1/2}.$$

At the defocus $\Delta z_B = 10\mu$, the $\Delta\rho$ value is mainly determined by the last term, which equals 17 nm for electrons with 100 keV energy.

The effect of the electron beam defocusing on $\Delta\rho(\mathbf{q}_f)$ can be seen in Fig. 5. For a perfect crystal, the intensity at point $\boldsymbol{\mu}_f = \lambda_0 f\mathbf{q}_f$ in the LACBED pattern depends on

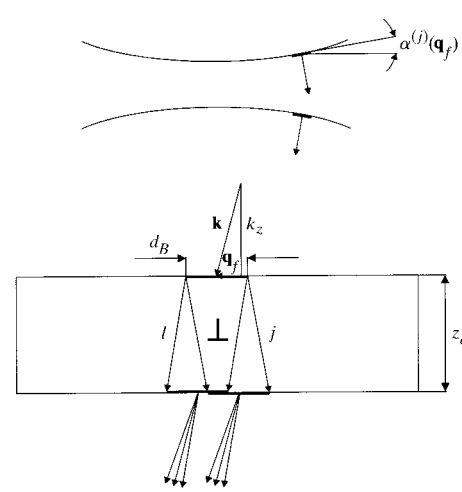

Fig. 4. Schematic diagram illustrating the transfer of the disturbances by the quasi-Bloch-wave packages in a crystal with a defect. After scattering in the crystal, only waves propagating in the direction of the transmitted beam are shown. The upper part of the figure shows the cross section of the dispersion surface with excited region. The arrows show the directions in which the quasi-Bloch wave transfers the disturbances.

the diffraction of the incident plane wave whose transverse component of the wave vector is equal to $\mathbf{q}_f$. In a crystal with a defect, the scattering of each wave produces a diffuse background. All the plane waves with the transverse component of the wave vector $\mathbf{q}_f$ contribute to the intensity of point $\boldsymbol{\mu}_f = \lambda_0 f \mathbf{q}_f$ in the LACBED pattern. The lateral size of the crystal region which affects the intensity of this point increases with increasing defocus $|\Delta z_B|$. The effect is fully neglected in simulating intensity according to formula (53) obtained with the use of the independent-plane-wave and column approximations. Within the framework of these approximations, the intensity of each point of the LACBED pattern is determined by scattering within the column, with a size of 2–3 nm.

It should be noted that errors produced by the independent-plane-wave approximation are not only dependent on the value of Δz_B but also on the speed of variations of the electron wave functions on the crystal exit surface. Indeed, when the variations of amplitudes $\varphi^{(j)}$ are slow, the effect of convolution in (55) can be neglected and (55) becomes equivalent to (53).

4.3. *LACBED patterns of a crystal with a dislocation*

As an example of the application of the developed theory, we simulated the LACBED patterns of a silicon crystal with an edge dislocation under incoherent illumination. Calculations were made for the transmitted beam of electrons with energy $E_0 = 100$ keV. Four systematic reflections of $(\bar{2}20)$ were included in the simulation. As shown in §2.2, scattering of quasi-Bloch waves in that case can be described with the use of the small-angle approximation and expression (51) can be applied.

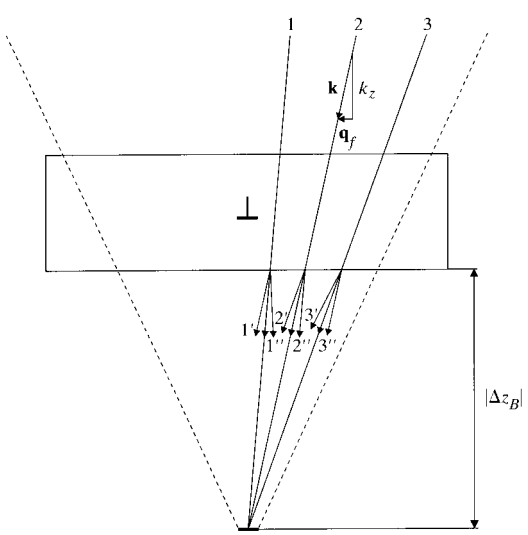

Fig. 5. Schematic view of the electron beam scattering in a crystal with a defect in LACBED. Wave 2 and diffuse waves $1'$ to $3''$ contribute to the intensity at point $\boldsymbol{\mu}_f = \lambda f \mathbf{q}_f$. The dashed lines show the limits of the illuminated cone.

Eigenvectors $[C^{(j)}]$ and eigenvalues $k_{0z}^{(j)}$ were determined by the program of Zuo, Gjonnes & Spence (1989), where the necessary changes were introduced. For the real and imaginary parts of the silicon potential, the data obtained by Radi (1970) and Weickenmeier & Kohl (1991) were used. The $0k_x$ axis was chosen along vector $\mathbf{g}_{\bar{2}20}$. To simplify the simulation, the dispersion surface curvature along the $0k_y$ axis was not taken into account, *i.e.* it was assumed that

$$\boldsymbol{\alpha}^{(j)}(\mathbf{p}) \simeq \boldsymbol{\alpha}^{(j)}(p_x, 0). \tag{56}$$

The well known expressions for the displacement field of a dislocation (Hirth & Lothe, 1982) were used. According to (51), the intensity $I_f(\boldsymbol{\mu}_f)$ is determined by the amplitudes $\varphi^{(j)}$ in the vicinity of point $\boldsymbol{\mu}_f = \lambda_0 \Delta z_B \mathbf{q}_f$. The values of $\varphi^{(j)}$ with steps $\Delta x = 1$ nm and $\Delta y = 1$ nm were found by the numerical integration of (22) using the fourth-order Adams method. Since approximation (56) was applied, for each value of y the amplitudes $\varphi^{(j)}$ were calculated at the nodes of the two-dimensional grid oriented along the $0x$ and $0z$ axes. The amplitude values between the grid nodes along the $0x$ axis were determined by a linear interpolation. The integration step was varied from $\Delta z = 0.1$ nm near the dislocation core to $\Delta z = 3.2$ nm at a distance from the core. After determining $\varphi^{(j)}$ values, integration of (51) was carried out by fast Fourier transformation.

Calculations were made using a personal computer with a Pentium 133 MHz processor. Simulating the LACBED pattern with a size of 70×70 points took about four hours. The developed calculation method can be extended to simulating images of the general displacement fields in the LACBED. It is also not difficult to include non-systematic reflections.

Figs. 6 and 7 show the LACBED patterns of an inclined dislocation. The patterns were calculated on the basis of both (51) and (53), with the use of independent-plane-wave and column approximations. The orientation of the crystal and that of the dislocation, and the specimen thickness are the same as in §2.2. Patterns in Figs. 6(*a*) and 7 were calculated using the same conditions, except for the sign of Δz_B, as were used by Wang *et al.* (1992) to obtain experimental and simulated LACBED patterns. The patterns labelled B in Figs. 6(*a*) and 7 are in good agreement with the simulation results of Wang *et al.* (1992).

In Figs. 6 and 7, the intensity distributions in patterns A and B are essentially different from each other in the vicinity of the dislocation image. Comparing patterns C and E in Figs. 6(*a*) and (*b*), one can see that with increasing $|\Delta z_B|$, errors in the case of the independent-plane-wave approximation increase in calculations both with or without the column approximation. As was noted in §4.2, the effect is caused by the increase of the

lateral size of the crystal region $\Delta\rho$ where scattering contributes to the intensity of each point in the LACBED pattern. Increase in $\Delta\rho$ influences such points in the diffraction pattern which correspond to the electron beam scattering in the defective region of the crystal near the dislocation.

The column approximation also results in errors in simulation. From patterns B and D in Fig. 6 and pattern B in Fig. 7, it is clear that the intensity distributions are symmetrical with respect to the straight line passing across the pattern centre normal to the $\bar{2}20$ reflection line. The symmetry is disturbed in the A patterns obtained without the column approximation. The symmetry disturbance is the result of the fact that because of the inclination of the dislocation the upper part of the dislocation image corresponds to the region of its intersection with the crystal entrance surface, while the lower part corresponds to the region at its intersection with the crystal exit surface. In §4.2, we noted that the accuracy of the column approximation depends on the distance between the dislocation core and the entrance surface of the specimen. Because of this dependence, the dislocation images in the A patterns are asymmetrical.

Fig. 7 shows the intensity distributions in LACBED patterns *versus* the dislocation distance from the zone axis. It can be seen that the differences between patterns A and B are qualitatively more pronounced in Figs. 7(*b*) and (*c*) than in Figs. 6(*a*) and 7(*a*). The dislocation images in the A patterns in Figs. 7(*b*) and (*c*) are much more blurred than those in the B patterns. This is mainly because in the patterns in Figs. 7(*b*) and (*c*) the intensity varies faster with the size at $\Delta\rho$ than in the patterns in Figs. 6(*a*) and 7(*a*). Therefore, the independent-plane-wave approximation ensures a lower accuracy in simulating the dislocation image. Comparison of the simulation result with the experimental patterns (Wang *et al.*, 1992) shows that the A patterns in Figs. 7(*b*) and (*c*) are in better agreement with experiments than the B patterns.

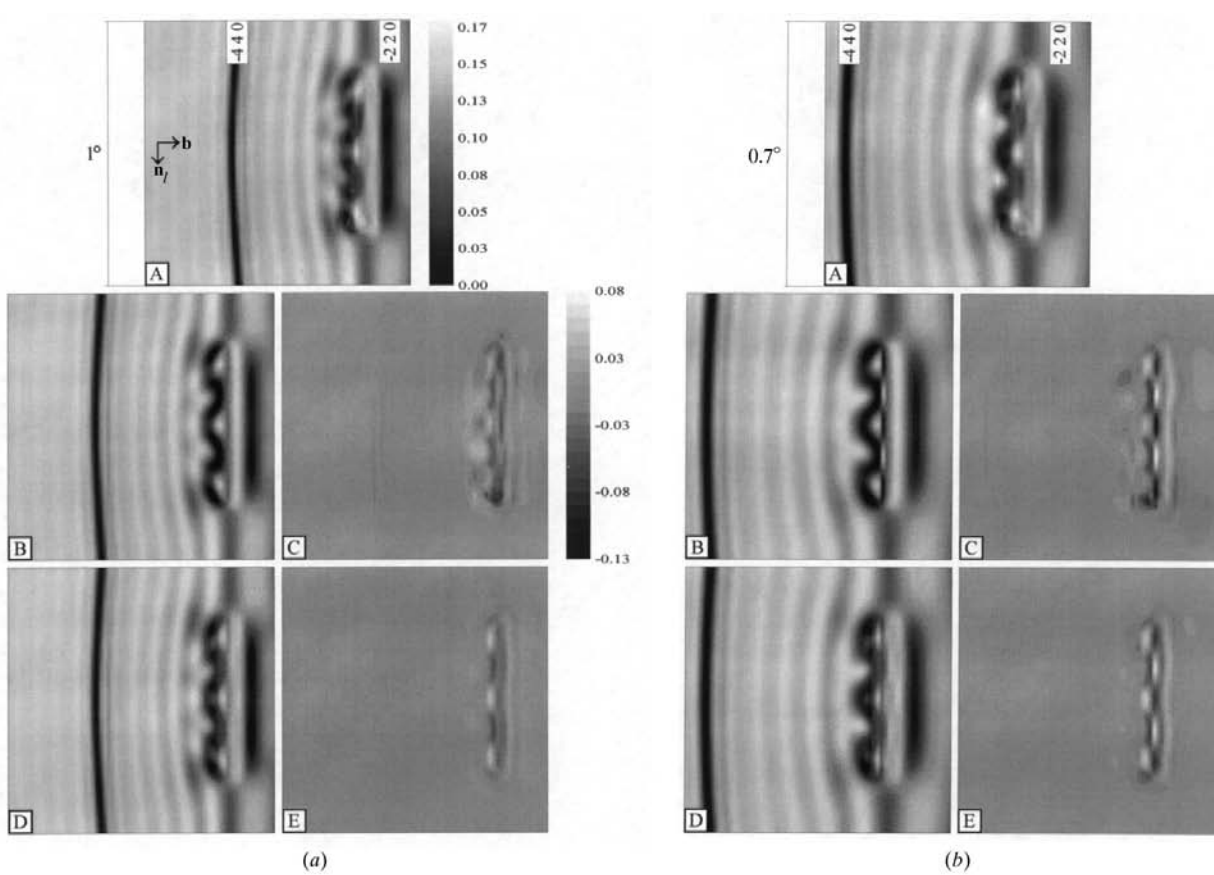

Fig. 6. Simulated LACBED patterns of a crystal with an inclined dislocation (*a*) at $\Delta z_B = -10\mu$ and (*b*) at $\Delta z_B = -14\mu$. The dislocation core projection onto the $0x$ axis is $x_d = 115$ nm distant from the origin. The A patterns are calculated with the use of the developed approach, the B patterns with the independent-plane-wave and column approximations, and the D patterns only with the column approximation. Patterns C and E are the differences between B and A, and B and D, respectively. The intensity is normalized so that without a specimen its value equals one at all the illuminated points in the diffraction pattern. In (*a*), the grey scale for patterns A, B and D is shown adjacent to A, while for patterns C and E it is adjacent to C. $\mathbf{n}_k = [111]$, $\mathbf{b} = \frac{1}{2}[\bar{1}10]$, $\mathbf{n}_l = [110]$, $z_e = 150$ nm.

When comparing the simulated and experimental patterns, one can also notice some shortcomings of the column approximation. In particular, the symmetry disturbances of regions α and β in the A pattern in Fig. 7(b) are well pronounced in the experimental LACBED patterns. As is seen from the B pattern in Fig. 7(b), using the column approximation does not result in the appearance of such asymmetry.

Thus, the results of simulation show that the developed approach allows a more accurate calculation of LACBED patterns than do approaches with the independent-plane-wave and column approximations.

5. Conclusions

To describe the dynamical diffraction of partially coherent electron beams by a crystal with a defect, the mutual coherency, the mutual intensity functions and formalism of quasi-Bloch wave have been used. An analytical expression correlating the mutual intensities on the exit and entrance surfaces of the crystal in terms of the scattering matrix has been obtained. The matrix elements describe the excitation of points on the branches of the dispersion surface after the plane incident wave being scattered. The elements can be found by solving the system of integro-differential equations determining the intrabranch and interbranch scattering of quasi-Bloch waves by the defect displacement field. The equations have been obtained without the column approximation, while the effect of the defect displacement field on the crystal potential has been taken into account by using the deformable ion approximation.

For many defects, *e.g.* dislocations, quasi-Bloch waves passing through the crystal are scattered at small angles. In that case, the scattering matrix elements can be found by solving the system of ordinary differential equations. The numerical integration of this system is not more difficult than the solution of equations for the amplitudes of quasi-Bloch waves obtained with the column approximation (Wilkens, 1964).

Mutual intensity on the entrance surface of the crystal has been found for the general case of defocused illumination by an incoherent source of electrons. An important case of incoherent illumination when the coherency length of the incident beam in the condenser

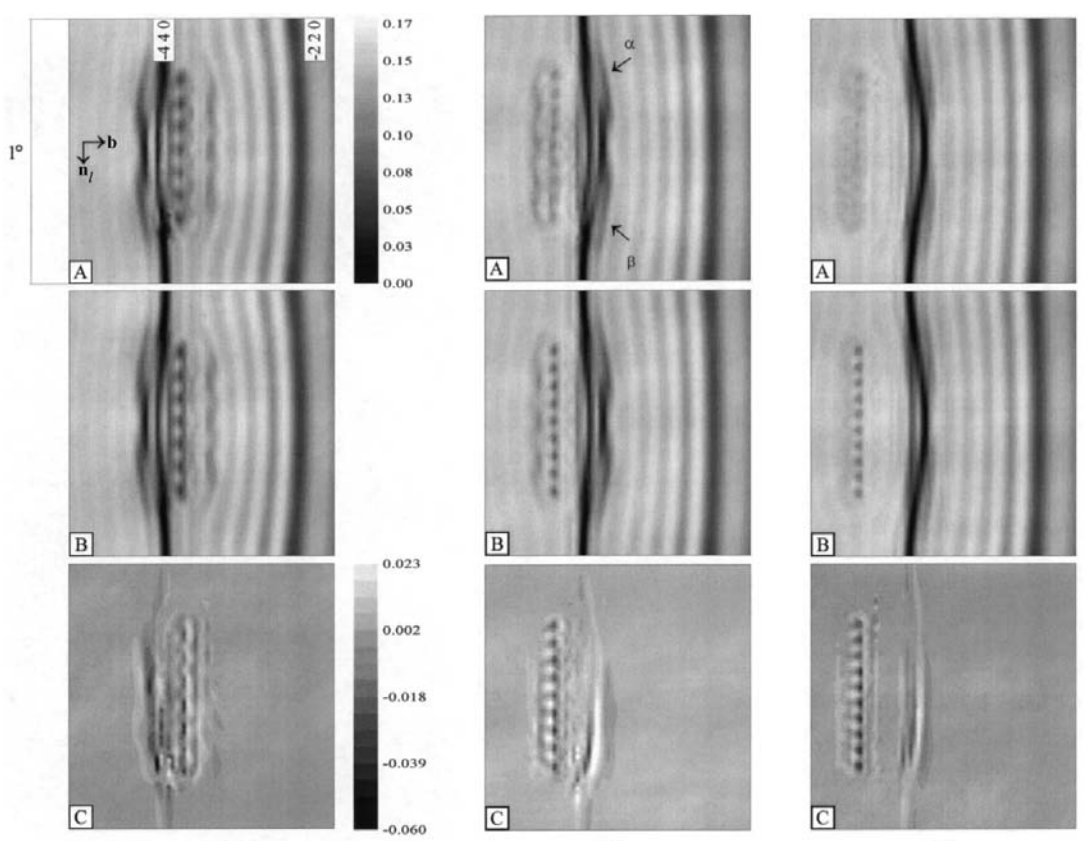

Fig. 7. Simulated LACBED patterns of a crystal with a dislocation at (a) $x_d = 178$ nm, (b) $x_d = 207$ nm and (c) $x_d = 221$ nm. The A patterns are calculated with the use of the developed approach, the B patterns with the independent-plane-wave and column approximations. The C patterns are the differences between B and A. $\Delta z_B = -10\mu$. The other details are the same as in Fig. 6.

diaphragm plane is many times smaller than the diaphragm size has been considered. Expressions for mutual intensity in the central region of the specimen illuminated area at various defocus Δz_B values have been obtained. It is shown that at large Δz_B the coherence length is inversely proportional to the angular size of the focused beam cross section, which is determined with respect to the cross point of the microscope optical axis with the specimen entrance surface. The effect of defocusing on the mutual intensity Fourier transform of the incident beam, determining the mutual intensity at the exit from the crystal has been found.

As an example of the application of the general theory, expressions for intensity on LACBED patterns under various illumination conditions have been obtained. The expressions made it possible to take into account the coherent properties of the incident electron beam and to describe its scattering by the crystal using only the deformable ion approximation for the lattice potential. Since the effect of the errors of that approximation on the intensity of LACBED patterns is weak, the expressions obtained can be used for simulation of images that are quantitatively comparable with the experimental ones. Calculations necessary for simulation are considerably reduced if the experimental images are obtained under incoherent illumination and the scattering of quasi-Bloch waves can be described with the use of the small-angle approximation.

For the case of incoherent illumination, it has been shown that the approximation of independent plane waves filling the illumination cone allows a correct determination of the intensity in LACBED patterns only at a small defocus of the electron beam. A formula for estimating the locality of the convergent-beam diffraction method when the displacement field in a crystal is investigated has been obtained. For CBED patterns, the locality is determined by the size of the electron beam on the specimen entrance surface, mutual orientation of the excited parts on the dispersion surface and the crystal thickness. In the LACBED patterns, the intensity at each point is dependent on the scattering conditions of the electron beam in the crystal region whose lateral size is about $2(2\lambda_0 \Delta z_B)^{1/2}$.

To demonstrate the theory, the LACBED patterns of a crystal with an inclined dislocation under incoherent illumination has been simulated. It has been found that the intensity distribution obtained with the new approach differs from that simulated with the use of the independent-plane-wave and column approximations. Causes of the shortcomings of those approximations have been analysed. Errors of conventional approximations increase with increasing $|\Delta z_B|$ or when the image of a dislocation becomes more distant from the zone axis. Comparison of simulated patterns with the experimental patterns obtained by Wang *et al.* (1992) shows that the developed approach allows a more exact description of the large-angle convergent-beam electron diffraction than do the independent-plane-wave and column approximations.

APPENDIX *A*

As shown by Borgardt (1993*b*), amplitudes $\psi^{(j)}$ for each value of E and i satisfy the equation

$$\sum_j \sum_g \int \left[k_{gz}^{(j)} \frac{\partial \psi^{(j)}}{\partial z} - \psi^{(j)} (2\pi i \mathbf{k}_g^{(j)} \cdot \nabla R_g - F) \right] \times C_g^{(j)} \exp(2\pi i \mathbf{k}_0^{(j)} \cdot \mathbf{r}) \exp(2\pi i R_g) \times \exp(2\pi i \mathbf{g} \cdot \mathbf{r}) \mathrm{d}\mathbf{p} = 0, \quad (57)$$

where $\mathbf{k}_g^{(j)} = \mathbf{k}_0^{(j)} + \mathbf{g}$, $F = \pi i (\nabla R_g)^2 - \frac{1}{2} \Delta \mathbf{R}_g$.

Quantity F is essential only when $\partial R_g / \partial z = 0$ and will be ignored for simplicity. Using the Fourier transformation, $\nabla R_g(\mathbf{r})$ can be presented in the form

$$\nabla R_g(\mathbf{r}) = \int \left(\mathbf{e}_z \frac{\partial}{\partial z} + 2\pi i \mathbf{p} \right) \tilde{R}_g(z, \mathbf{p}) \exp(2\pi i \mathbf{p} \cdot \boldsymbol{\rho}) \, \mathrm{d}\mathbf{p}. \quad (58)$$

Substituting (58) into (57), we obtain

$$\sum_g \int \left\{ \sum_j \left(k_{gz}^{(j)}(\mathbf{p}) \frac{\partial \psi^{(j)}(z, \mathbf{p})}{\partial z} C_g^{(j)}(\mathbf{p}) \exp[2\pi i k_{0z}^{(j)}(\mathbf{p}) z] - 2\pi i \int \psi^{(j)}(z, \mathbf{p}') C_g^{(j)}(\mathbf{p}') \exp[2\pi i k_{0z}^{(j)}(\mathbf{p}') z] \times \left[k_{gz}^{(j)}(\mathbf{p}') \frac{\partial}{\partial z} + 2\pi i (\mathbf{p}' + \mathbf{g}_p) \cdot (\mathbf{p} - \mathbf{p}') \right] \times \tilde{R}_g(z, \mathbf{p} - \mathbf{p}') \mathrm{d}\mathbf{p}' \right) \right\} \exp(2\pi i \mathbf{p} \cdot \boldsymbol{\rho}) \exp(-2\pi i R_g) \times \exp(2\pi i \mathbf{g} \cdot \mathbf{r}) \, \mathrm{d}\mathbf{p} = 0. \quad (59)$$

Since the terms in braces are independent of $\boldsymbol{\rho}$, expression (59) is satisfied when each term is equal to zero,

$$\sum_j \left\{ k_{gz}^{(j)}(\mathbf{p}) \frac{\partial \psi^{(j)}(z, \mathbf{p})}{\partial z} C_g^{(j)}(\mathbf{p}) \exp[2\pi i k_{0z}^{(j)}(\mathbf{p}) z] - 2\pi i \int \psi^{(j)}(z, \mathbf{p}') C_g^{(j)}(\mathbf{p}') \exp[2\pi i k_{0z}^{(j)}(\mathbf{p}') z] \times \left[k_{gz}^{(j)}(\mathbf{p}') \frac{\partial}{\partial z} + 2\pi i (\mathbf{p}' + \mathbf{g}_p) \cdot (\mathbf{p} - \mathbf{p}') \right] \times \tilde{R}_g(z, \mathbf{p} - \mathbf{p}') \mathrm{d}\mathbf{p}' \right\} = 0. \quad (60)$$

Hitherto, we have not imposed any limitations upon the eigenvectors $[C^{(j)}]$. If they are determined by the solution of the eigenvalue problem with a complex potential, equations for the amplitudes $\psi^{(j)}$ can be obtained using the matrix form of (60). If absorption in the crystal is taken into account by the perturbation method and the eigenvalues are calculated with the use

of the real part of the potential, then coefficients $C_g^{(j)}$ satisfy the normalization condition (Jones *et al.*, 1977)

$$\sum_g C_g^{(j)}(\mathbf{p}) C_g^{(l)*}(\mathbf{p})(1 + g_z/K_0) = \delta_{jl}, \tag{61}$$

where δ_{jl} is the Kronecker symbol.

We restrict ourselves to considering the second case. For $k_{gz}^{(j)}(\mathbf{p})$ that are not included in the exponential functions, we assume that

$$k_{gz}^{(j)}(\mathbf{p}) \simeq k_{gz}^{(l)}(\mathbf{p}) \simeq K_{gz}(\mathbf{p}). \tag{62}$$

Multiplying the gth equation of the system (60) by $C_g^{(l)*}(\mathbf{p})(1 + g_z/K_0)$, we sum up all equations and, taking into account (61) and (62), we obtain equation system (7).

References

Bird, D. M. & Preston, A. R. (1988). *Phys. Rev. Lett.* **61**, 2863–2866.

Bithell, E. G., Donovan, P. E. & Stobbs, W. M. (1989). *Philos. Mag.* A**59**, 63–85.

Borgardt, N. I. (1993*a*). *Crystallogr. Rep.* **38**, 725–729.

Borgardt, N. I. (1993*b*). *Philos. Mag.* A**68**, 453–470.

Borgardt, N. I. (1995). *Crystallogr. Rep.* **40**, 206–210.

Borgardt, N. I. (1996). *Acta Cryst.* A**52**, 898–908.

Born, M. & Wolf, E. (1968). *Principles of Optics*. Oxford: Pergamon Press.

Carpenter, R. W. & Spence, J. C. H. (1982). *Acta Cryst.* A**38**, 55–61.

Chou, C. T., Preston, A. R. & Steeds, J. W. (1992). *Philos. Mag.* A**65**, 863–888.

Coene, W., Van Dyck, D. & Van Landaut, J. (1986). *Optik (Stuttgart)*, **73**, 13–18.

Fejes, P. L. (1977). *Acta Cryst.* A**33**, 109–113.

Frank, J. (1973). *Optik (Stuttgart)*, **38**, 519–536.

Goodman, J. W. (1985). *Statistical Optics*. New York: John Wiley.

Hawkes, P. W. (1978). *Adv. Opt. Electron Microsc.* **7**, 101–184.

Hirsch, P. B., Howie, A., Nicholson, R. B., Pashley, D. W. & Whelan, M. J. (1965). *Electron Microscopy of Thin Crystals*. London: Butterworths.

Hirth, J. P. & Lothe, J. (1982). *Theory of Dislocations*. New York: John Wiley.

Humphreys, C. J. & Spence, J. C. H. (1981). *Optik (Stuttgart)*, **58**, 125–144.

Ishizuka, K. (1980). *Ultramicroscopy*, **5**, 55–65.

Jones, P. M., Rackham, G. M. & Steeds, J. W. (1977). *Proc. R. Soc. London Ser. A*, **354**, 197–222.

Katerbau, K.-H. (1981). *Philos. Mag.* A**43**, 409–426.

Landau, L. D. & Lifshitz, E. M. (1977). *Quantum Mechanics, Non-Relativisitic Theory*. Oxford: Pergamon Press.

Lu, G., Wen, J. G., Zhang, W. & Wang, R. (1990). *Acta Cryst.* A**46**, 103–112.

Maier, H. J., Keller, R. R., Renner, H., Mughrabi, H. & Preston, A. (1996). *Philos. Mag.* A**74**, 23–43.

Pozzi, G. (1987). *Optik (Stuttgart)*, **77**, 69–73.

Rose, H. (1984). *Ultramicroscopy*, **15**, 173–192.

Radi, G. (1970). *Acta Cryst.* A**26**, 41–56.

Spence, J. C. H. & Carpenter, R. W. (1986). *Principles of Analytical Electron Microscopy*, edited by D. C. Joy, A. D. Romig Jr & J. I. Goldstein, pp. 301–352. New York: Plenum Press.

Spence, J. C. H. & Zuo, J. M. (1992). *Electron Microdiffraction*. New York: Plenum.

Wade, R. H. & Frank, J. (1977). *Optik (Stuttgart)*, **49**, 81–92.

Wang, S. Q., Peng, L. M., Xin, Y., Chu, Y. M. & Duan, X. F. (1992). *Philos. Mag. Lett.* **66**, 225–233.

Wei, X., Duan, X. F. & Wang, S. Q. (1996). *Ultramicroscopy*, **66**, 49–57.

Weickenmeier, A. & Kohl, H. (1991). *Acta Cryst.* A**47**, 590–597.

Wilkens, M. (1964). *Phys. Status Solidi*, **6**, 939–956.

Zuo, J. M., Gjonnes, K. & Spence, J. C. H. (1989). *J. Electron Microsc. Tech.* **12**, 29–55.

Zuo, J. M. & Spence, J. C. H. (1993). *Philos. Mag.* A**68**, 1055–1078.